



TECHNISCHE  
UNIVERSITÄT  
WIEN

# Master Thesis

## Optimisation of processing parameters of a laboratory extrusion press for the application in Aluminium alloys

carried out for the purpose of obtaining the degree of Dipl.-Ing., submitted  
at TU Wien, Faculty of Mechanical and Industrial Engineering, by

**Martin Ziegler, BSc**

Mat.Nr.: 00930687

under the supervision of

**Ass. Prof. Dr. sc. ETH Erwin Povoden-Karadeniz**

E308

Institute of Materials Science and Technology

Vienna, March 2019

Signature

A handwritten signature in blue ink, appearing to be 'Erwin Povoden-Karadeniz', written over a light blue horizontal line.

## **Abstract**

Extrusion of aluminium alloys, especially the 6xxx alloys, is a widely used industrial process to manufacture lightweight products of complex geometries. There are numerous process parameters that have an impact on end product quality. The goal of this thesis is to optimize the essential parameters for a laboratory extrusion press in order to generate a whole process chain that allows scaled down production as a reference to industrial processes and as an efficient source for the extraction of input parameters for microstructural modelling.

In an experimental series with billets of AW6082 alloy, heating characteristics of the laboratory oven prior to extrusion were tested and a pre-heating routine for the billets is established. Four different die geometries were tested on their functionality. Their effectiveness for a fine microstructure and their extrusion ratios were evaluated. The microstructure of extrudates was analysed using light optical microscopy. Furthermore, the influence on hardness of different thermal treatments after extrusion was evaluated. It could be shown, that variation of billet pre-heating in a temperature range from 420 to 540°C has only a minor impact on end product hardness, but that a subsequent solution annealing and artificial ageing step increases Brinell hardness significantly.

## Kurzfassung

Das Strangpressen von Aluminiumlegierungen, speziell die der 6xxx-Serie, ist ein weit verbreiteter industrieller Prozess um Leichtbauprodukte komplexer Geometrien herzustellen. Eine Vielzahl an Prozessparametern wirken sich auf die schlußendliche Produktqualität aus. Ziel dieser Arbeit ist es, die essentiellen Parameter der Laborstrangpresse zu optimieren und so eine vollständige Prozesskette zu erschaffen, mit der eine Produktion im Labormaßstab ermöglicht wird die einen Vergleich zu industriellen Standards zulässt und außerdem eine Quelle für Input-Variablen zur Gefüge-Simulation bietet.

In experimentellen Tests mit Bolzen der Legierung AW6082 konnte die Aufheizcharakteristik des Laborofens untersucht und eine Routine für die Bolzen-Vorwärmung etabliert werden. Vier unterschiedliche Werkzeuggeometrien wurden auf deren Funktionalität überprüft. Deren Effektivität um eine über den Querschnitt gleichmäßig verteilte Mikrostruktur zu schaffen wurde untersucht und deren Verpressungsverhältnisse wurden evaluiert. Das Gefüge der Extrusionsprodukte wurde lichtmikroskopisch analysiert. Weiters wurde der Einfluss verschiedener nachfolgender Wärmebehandlungen auf die Härte evaluiert. Es konnte gezeigt werden, dass eine Variation der Bolzenvorwärmung im Temperaturbereich von 420 bis 540°C nur geringe Auswirkungen auf die Endhärte hatte, dass jedoch eine nachfolgende Lösungsglühung mit Warmauslagerung die Brinellhärte deutlich anhob.

## **Acknowledgements**

I would like to show my gratitude to some people, who made the time as a student at TU Wien, and especially the time during which this thesis was written, a very special one:

Most of all, I want to thank Erwin Povoden-Karadeniz for his competent and supportive guidance and supervision throughout the time of the thesis. He was truly inspiring and showed me the scientific way to handle such a challenging topic. Also I want to thank Bernhard Miesenberger, who was the mastermind in planning and conducting all the experiments and helped me a lot with his expertise and wisdom.

Furthermore, I would like to thank the project partners CDL-IPE and Neuman Aluminium Strangpresswerk GmbH for giving me the chance to write my master thesis in such an amazing and fascinating field of technology. Particularly Andreas Pasching and Andreas Niederer had plenty of valuable input and support for me.

Furthermore, I want to thank all the people from the Institute of Materials Science and Technology of TU Wien, who made it such an enjoyable time at the department and a great place to work at.

Last but not least, a big thanks goes out to my friends Paul, Zmoe and Patrick and my family Renate, Elisabeth, Andrea and Werner for their invaluable support throughout my whole academic career and beyond.

## Table of contents

1	Introduction .....	1
2	Objectives .....	3
3	State of the art.....	4
3.1	Alloying elements of AW6082 .....	4
3.1.1	The Al-Mg-Si subsystem.....	5
3.1.2	Multi-component extensions based on Al-Mg-Si .....	6
3.1.3	Excess of Silicon .....	8
3.2	Precipitation Hardening .....	10
3.2.1	Ageing .....	11
3.3	Recrystallization and coarse grain .....	13
3.4	Extrusion process .....	15
3.4.1	Casting .....	16
3.4.2	Homogenization .....	17
3.4.3	Pre-heating .....	19
3.4.4	Extrusion.....	19
3.4.5	Artificial Ageing .....	26
4	Experimental .....	27
4.1	Extrusion press and handling.....	27
4.1.1	Furnace setup.....	27
4.1.2	Furnace – press transition .....	28
4.1.3	Extrusion press and cooling .....	29
4.2	Die geometries.....	31
4.3	Thermal routes.....	33
4.4	Analyses of microstructure.....	34
	Etching: .....	36
4.5	Hardness testing.....	36

5	Results and discussion .....	38
5.1	Pre-heating characteristic of billets .....	38
	Error of furnace and thermocouples:.....	40
	Calculation of pre-heating time:.....	43
5.2	Calculation of extrusion exit temperature.....	45
5.3	Evaluation of extrusion ratio and strain rate.....	47
5.4	Influence of die geometry on the extrudate microstructure .....	50
	Stretching of grains: .....	51
5.5	Influences of different thermal routes.....	53
5.6	Dispersoids .....	57
6	Summary and Conclusions .....	59
7	Outlook.....	60
8	References.....	62
	List of figures .....	64
	List of tables .....	66

## 1 Introduction

As a metal of relatively low density (2,7 g/cm<sup>3</sup>), aluminium and its alloys have a wide use of application, especially for lightweight construction, such as transportation and aircraft but also for building and construction, packaging as cans or foils or in electrical industries. Approximately 75 – 80% of aluminium is used for wrought products, i.e. products are produced from cast ingots with a subsequent metal forming step, resulting in manufactures such as rolled plate, sheet, foil, extrusions, rod, bar, tube or wire [1].

Aluminium alloys are in direct competition to other lightweight metals, mainly magnesium or titanium but have the advantage of their wide variability in application, their good formability in hot- and cold-working, corrosion resistance, good recyclability, mid- to high strength and of course the comparatively small price. While pure aluminium of 1xxx-series is soft, alloys of 6xxx-series gain a tensile strength of up to 410 N/mm<sup>2</sup> in T6<sup>1</sup> tempering [2]. The digit at the beginning of the series-code designates the main alloying elements of the Al-alloy, according to standard DIN EN 573-1 [3], as shown in Table 1. For extrusion mainly alloys of series 2xxx, 6xxx and 7xxx are used, in which especially 6xxx-group alloys are favoured for many applications. Those alloying groups gain their good strength and hardness from their solution hardenability. For 6xxx-alloys those hardening phases are Mg- and Si-containing particles in the nanometres range, which are finely precipitated in the aluminium matrix and thus build a barrier for dislocation movement.

**Table 1: Numerical designation system for Al-alloys [3] [4].**

<b>Group</b>	<b>Main alloying elements</b>	<b>Hardenability</b>
<b>1xxx</b>	min. 99% Al	No
<b>2xxx</b>	Cu	Yes
<b>3xxx</b>	Mn	No
<b>4xxx</b>	Si	No

<sup>1</sup> According to Standard DIN EN 515 [32], T designates a heat treatment of material so that any other state is achieved than F, O or H. The first digit behind T indicates the sequence of treatments.

T6...Solution annealed followed by artificial ageing.

<b>5xxx</b>	Mg	No
<b>6xxx</b>	Mg + Si	Yes
<b>7xxx</b>	Zn	Yes
<b>8xxx</b>	Other elements	No
<b>9xxx</b>	Not used yet	-

One of the most utilized and manufactured alloys inside the 6xxx-group is the aluminium wrought (AW) alloy AW6082. This alloy contains Si in a range of 0,7 – 1,3 and Mg of 0,6 – 1,2 weight percent. The main forming process for this material is hot extrusion. Aside from casting, extrusion is the most economic process for forming aluminium. There are no other construction materials, that can be as easily and as economically formed in such complex cross-sectional geometries as with the extrusion process [4]. The biggest market segment for aluminium extrusion is building and construction, where extrudates are used in doors, windows, panels, frames, ladders and so on.

From an industrial point of view, an increase in productivity and decrease of costs are desirable. Increasing productivity goes hand in hand with increasing speed of extrusion, i.e. ram speed but this is limited by quality requirements of the end product. Costs are essentially produced by energy consumption of the press, meaning that resistance during the pressing process should be kept at a minimum. Pressing resistance is strongly influenced by the flow stress of the material, which depends on alloying elements and thermal homogenization routine prior to extrusion.

Among the numerous parameters that influence end product quality throughout the whole extrusion process, the focus in this thesis is put on the basic parameters pre-heating of billet, ram speed and die geometry. The long-term goal based on the results of this thesis is to establish a functioning process chain of the laboratory press, consisting of a pre-heating-, extrusion- and tempering-step. This will enable easy, cheap and efficient tests of parameter sets and / or alloying compositions serving as input parameters for microstructural modelling and simulations and assisting the advancement of industrial extrusion. Testing and optimizing parameters of an industrial scale extrusion press often comes along with high costs, downtimes of the machines and therefore loss of production or unknown material quality output. Hence, an easy way to minimize risks is to test changes in parametrisation on a laboratory extrusion press.

## 2 Objectives

The goal of this thesis is to investigate the role of process parameters through characterisation of the microstructure and to establish a reproducible pressing routine for a laboratory 2 MN (maximum press force) extrusion press. The whole extrusion process should be optimised regarding a homogenous texture and grain size throughout extrudates cross-section, which is expected to improve mechanical properties. Hardness tests of artificially aged extrudates should be conducted. Therefore, the influence of the following parameters were investigated:

- Pre-heating temperatures of billets
- Influence of ram speed
- Functionality of different dies and die geometries and their influence on extrudate microstructures in terms of grain sizes and grain distribution
- Quenching rates for extruded products
- Heat treatment following the extrusion

### 3 State of the art

#### 3.1 Alloying elements of AW6082

The wrought alloy AW6082 is of medium strength (an extruded bar in T6 condition has a tensile strength of 310 N/mm<sup>2</sup> [2]), high fracture toughness and has excellent corrosion resistance. Furthermore, it shows good weldability, machinability and cold working qualities. The chemical composition of the billets used for extrusion is given in Table 2, according to standard of alloying elements [5]. Within this composition range, the specific alloy especially contains a high content of Si.

Table 2: Composition of EN AW6082 billets in weight percent.

AW6082	Si	Fe	Cu	Mn	Mg	Cr	Zn	Ti
Standard	0,7 – 1,3	0,5	0,1	0,4 – 1,0	0,6 – 1,2	0,25	0,2	0,1

Alloying elements have different impacts on extrudability or end product properties, so it is important to understand their role in the context of the process. All these process parameters like temperatures, heating and cooling rates are influenced by the composition. For example, Mg and Si are added to form the hardening phase Mg<sub>2</sub>Si and increase yield strength. To gain the desired strength it is essential to bring the Mg<sub>2</sub>Si-phase in solution at elevated temperature during extrusion or at a subsequent solution annealing step. The maximum temperature is limited though, because incipient melting of eutectic phases at the surface needs to be avoided. Also, if Mg and Si are entirely in solution before the extrusion step they increase the flow stress, thus making the billet tougher to extrude [6].

Another example is Mn or Cr, which form intermetallic compounds (dispersoids) during homogenization. They influence the recovery, recrystallization and grain growth behaviour. Once again, the formation and structure of these phases is strongly connected to the composition, specific heating and cooling rates [7]. The recrystallization behaviour and growth of coarse grain is a known issue in aluminium extrusion and strongly affects a uniform end product quality.

Typical heat treatments in an industrial extrusion plant are homogenization, to improve extrudability and overall material properties (dissolve Mg<sub>2</sub>Si precipitates and coarse eutectics, remove dendritic segregation, create a more homogenous structure) and precipitation hardening (solution annealing and ageing) to increase strength [6]. For a rough evaluation of these

temperature ranges the pseudo-binary Al-Mg<sub>2</sub>Si equilibrium phase diagram in Figure 1 can be used, representing one relevant base system of AW6082.

### 3.1.1 The Al-Mg-Si subsystem

AlMgSi-alloys of high purity consist of two phases at thermal equilibrium. The  $\alpha$ -phase denoting the face-centred cubic (fcc) Al-solid solution matrix and the intermetallic Mg<sub>2</sub>Si compound  $\beta$ -phase (also fcc). The Al-Mg<sub>2</sub>Si system has an eutectic point at 13,9 weight percent Mg<sub>2</sub>Si, with a pseudo-eutectic temperature at 594°C respectively. The maximum solid solubility for Mg<sub>2</sub>Si in fcc Al is at 1,91 weight percent Mg<sub>2</sub>Si at 583,5°C [4]. Solubility of Mg and Si in the matrix strongly decreases with decreasing temperature and only measures 0,08 wt.% at 200°C [4]. A feature of tremendous technological relevance is the high potential for kinetic stabilisation of metastable Si-Mg- clusters and intermetallic phases of the AlMgSi system. Some of these phases can also form in the framework of extrusion process of AW6082.

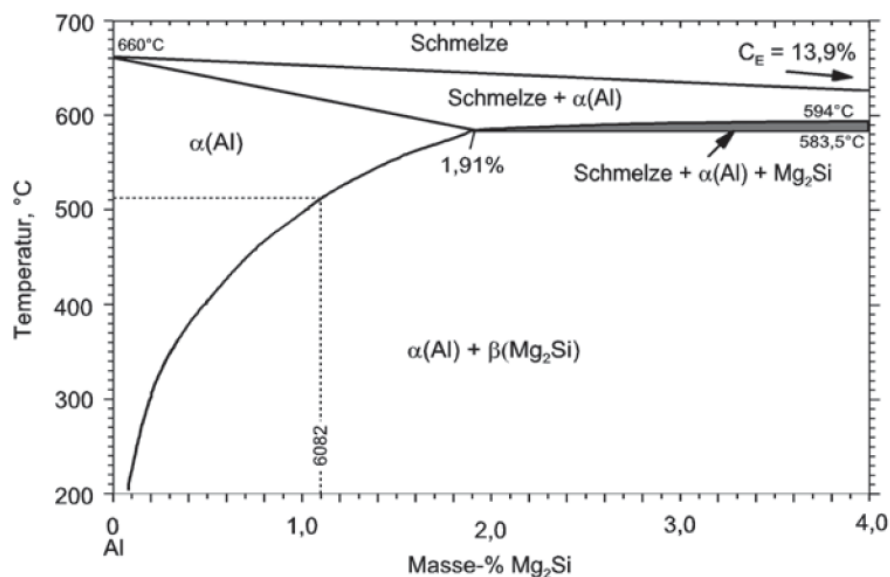


Figure 1: Quasi-binary phase diagram for AlMgSi-alloys [4].

It is mandatory to add a minimum amount of Si and Mg to the alloy, so that the required strength in T6 temper can be achieved. On the other hand, increasing amounts of those elements have a negative effect on extrusion by increasing extrusion pressure and reducing extrusion speed [8]. However, industrial alloys such as the AW6082 contain an excess of Si, so that sufficient stoichiometric Mg<sub>2</sub>Si-phases can form for precipitation hardening [9]. In case of an excess of Si

(see also section 0) the weight percentage of Mg<sub>2</sub>Si-phases built can be calculated on the basis of Mg contents [10]:

$$Mg_2Si_{wt.\%} = Mg_{wt.\%} + 0,578 \cdot Mg_{wt.\%} = 1,578 \cdot Mg_{wt.\%} \quad (1)$$

The factor of 0,578 in equation (1) originates from the ratio of atomic masses from Si to twice from the one of Mg. For the given alloy, this yields 1,33 wt.% of Mg<sub>2</sub>Si. In a first approximation for the understanding of the temperature-dependent phase equilibria in AW6082 (neglecting possible effects of alloying elements other than Mg and Si), Figure 1 can be used.

### **3.1.2 Multi-component extensions based on Al-Mg-Si**

In fact, when multi-component thermodynamic databases are available, it is indicative to compute phase equilibria of technological, extended compositions in phase fractions versus temperature. Simulation with the program *MatCalc* involving the thermodynamic multi-component database *mc\_al* is shown in Figure 2. For the simulation, the specific alloying composition according to standard was used (see Table 2). The simulation shows a dissolution temperature for Mg<sub>2</sub>Si of 570°C and a solidus temperature of 584°C, which leaves a very small temperature window for solution of Mg and Si. Solution of these elements is desired during homogenization and then again, either at the end of extrusion or in a subsequent solution annealing step, so that finely dispersed precipitates for the age hardening could be formed. It is preferred, that these elements dissolve during extrusion, making a subsequent solution annealing redundant and thus saving process time and energy. Even if the material is heated above the dissolution temperature, not all Mg and Si particles will be in solution and disposable to build the Mg<sub>2</sub>Si equilibrium phase and its precursors thereafter. This is mainly because parts of Si is also bound in dispersoid building phases, namely AlFeSi and Al(Fe,Mn)Si, which will only dissolve at higher temperatures

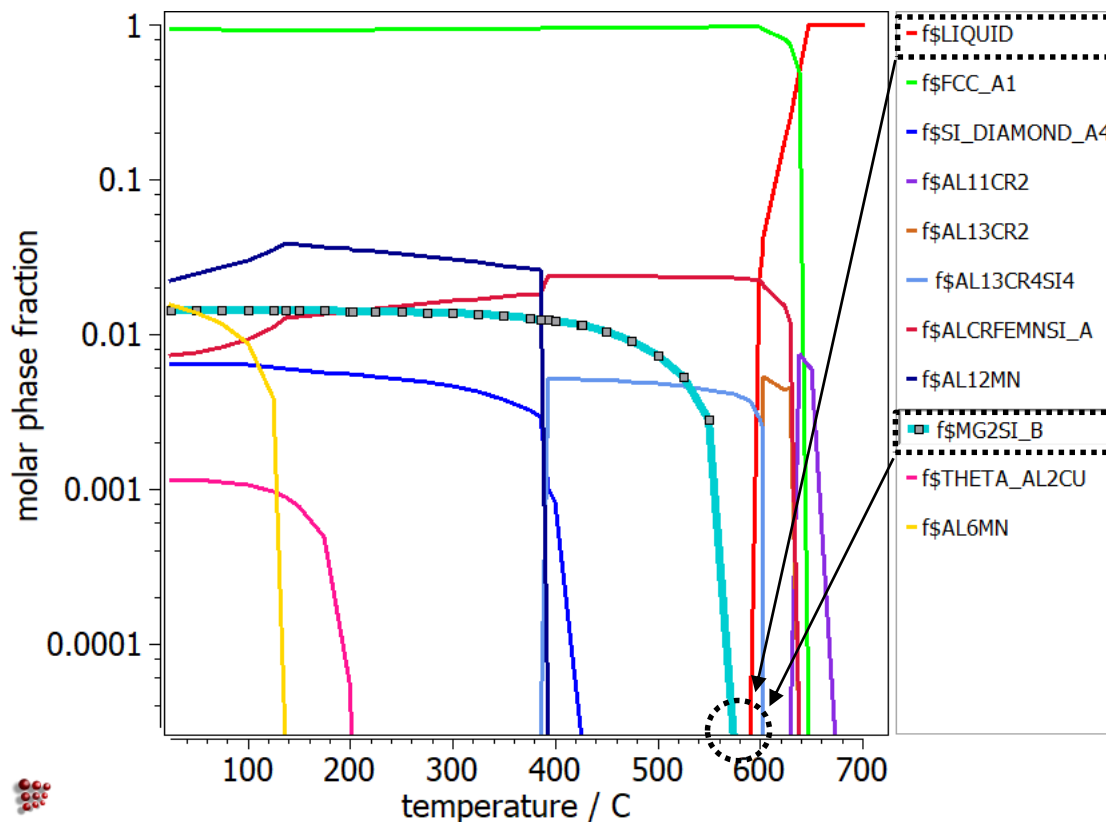


Figure 2: *MatCalc* thermodynamic equilibrium computation of specific AW6082 alloy. The black dotted circle marks the temperature window where Mg-Si intermetallic phases are dissolved into solid solution.

Due to relatively low solubility, even low Fe contents have a noticeable impact on the alloy microstructure. Fe-containing intermetallic phases (e.g.  $\text{Al}_8\text{Fe}_2\text{Si}$ ,  $\text{Al}_5\text{FeSi}$ ,  $\text{Al}_8\text{FeMg}_3\text{Si}_6$ ) can precipitate during solidification process, representing so-called primary phases. Those coarse and needle-like  $\text{AlFeSi}$ -phases are thermally resistant and thus their composition, fraction and morphology barely changes in the temperature range from  $500^\circ - 550^\circ\text{C}$ . However, it is possible to receive better ductility by homogenizing at higher temperatures, which results in globular spheroidizations due to structural changes among the series of  $\text{AlFeSi}$ -phases [4].

The important alloying elements Mn and Cr in AW6082 also possess small solubilities in fcc-Al and contribute to second phase formations in the matrix. Particularly, they seem to promote secondary dispersoid formation during the heating step at homogenization and stabilise these phases after homogenizing. Controlling dispersions has high significance within the extrusion process. Secondary dispersoids can efficiently delay recrystallization (Zener-drag), by pinning interfaces and therefore stabilizing the hot forming structure during extrusion and avoiding the formation of coarse grain.

On the downside, higher contents of dispersoid-building particles (Mn and Cr) increase quenching sensitivity of the material, because early precipitation of Si- and Mg-particles is more likely to happen on the mentioned dispersoid phases when quenching rates are too low. Precipitated Si-particles are no longer available to build hardening phases, resulting in a decrease of mechanical properties. Thus alloys with a high content of Mn and Cr require fast cooling rates after solution annealing or homogenization [4].

Furthermore, dispersoids may just have a minor influence on strength at room temperature but they do have a great influence on flow stress at higher temperatures, affecting extruding and productivity characteristics [4].

### **3.1.3 Excess of Silicon**

As can be seen, Si is the main alloying element in AW6082, followed by Mg and Mn. Mg is added so that Mg-Si strengthening precipitates can form under controlled heat treatments.

In Figure 3 compositions of some 6xxx alloys are shown. The figure shows the stoichiometric line for  $Mg_2Si$ , the limit of excess Si, which indicates, that many of the established 6xxx alloys possess excess Si (right side of stoichiometric line). In principle, excess of Si increases yield strength after ageing considerably due to enhanced formation of strengthening precipitates. Simulations revealed the coupled thermodynamic and quenched vacancies control of an increased number density of metastable  $\beta''$  particles (stoichiometric composition is  $Mg_5Si_6$ , see section 0), which is considered to be the main hardening phase [11].

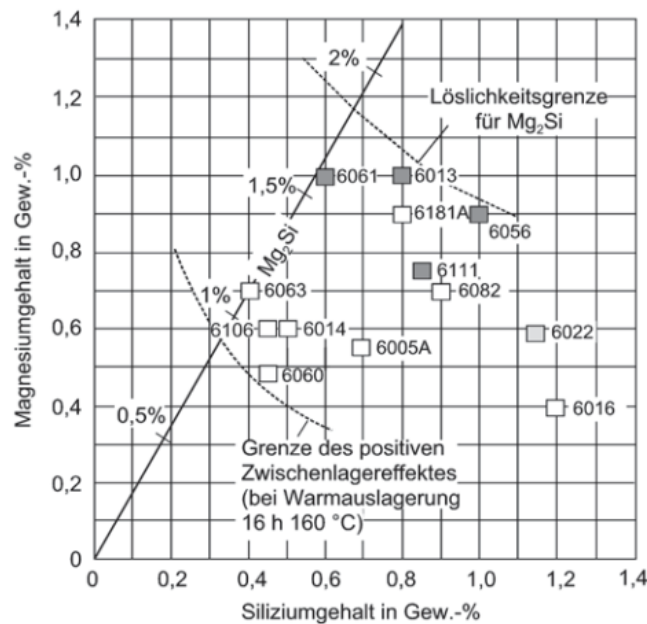


**Figure 3: Mg- and Si- contents for many 6xxx alloys. Empty box means no Cu in the alloy, filled box indicates Cu content [4].**

In the framework of extrusion process, Tomovic-Petrovic and Jensrud [8] showed in their studies, that an enhanced Si-level reduces the extrudability compared to standard AW6082 alloy. The authors cast, homogenized and extruded 3 different alloying compositions, containing nearly 2, 3,7 and 5,5 weight percent of Si. The extrusion speed was limited because of hot tearing on the extrudates' surface. Furthermore, mechanical properties of T6 tempering were below those of standard alloying composition. On the other hand, they showed, that an excess of Si has no impact on extrusion pressure. According to them, increasing Si contents in 6xxx wrought alloys would be beneficial for recyclability, since composition tolerances in alloy production are widened.

The negative influence of Si on extrudability was also shown by Reiso [12]. Assuming that Mg and Si are in solid solution during extrusion (because of homogenization practice and reheating), hot tearing on the extrudate surface occurs when the extrusion exit temperature gets close to the solidus temperature, which is determined by alloying components and is decreasing with increasing Mg and Si contents (see Figure 1). At the same time deformation resistance is increasing, resulting in heat generation (also see section 0) and promoting hot tearing. Furthermore, higher contents of Mg and Si bare the risk of early precipitation of  $Mg_2Si$  particles prior to extrusion. Extrudability is reduced by limited maximum temperature due to onset of melting of eutectic phases [12].

In addition, the alloy is more sensitive to quenching conditions when particles are dissolved after a heating step. With increased  $Mg_2Si$  content, excess of Si and increased volume fraction of dispersoid building particles, the quenching rate must also be increased to avoid early precipitation of the  $Mg_2Si$  equilibrium phase and its precursors. If cooling rates are too low, there are not enough precipitates in the super saturated solution to form the needed  $\beta''$  hardening phase during artificial ageing and therefore meet the required mechanical properties according to standard conditions.

Moreover, excess Si tends to segregate as coarse Si-particles at grain boundaries, which has a negative impact on ductility and enhances intergranular fracture. This crystallisation of Si particles can be countered, though, by adding dispersoid building elements (Fe, Mn) or homogenizing of material [4].

### 3.2 Precipitation Hardening

Precipitation hardening is a heat treatment method for increasing yield strength of temperable alloys. Precipitates in the nanometres-scale are barriers for dislocation movement, thus give a rise in strength as well as in resistance against plastic deformation. In Al-alloys based on Al-Mg-Si, controlled tempering after solution annealing and quenching produces finely distributed metastable strengthening Mg-Si precipitates. The temperature range for solution annealing should be between the dissolution temperatures of expected strengthening precipitates and the solidus temperatures for a given concentration. According to Figure 2, the  $\beta$ -phase for this alloy completely dissolves at  $570^\circ C$ . Usually annealing temperature is kept a bit lower, in a temperature range from  $510^\circ C$  to  $540^\circ C$  to not exceed eutectic temperature. This is to avoid partial melting of material zones due to enrichment of alloying elements with a lower melting point. Annealing time depends on several factors such as maximum temperature, texture, alloying elements (and related diffusion mobilities) or physical dimension of the ingot. Solution annealing is completed, when enough Mg- and Si-particles for precipitation are dissolved in the matrix to show an age-hardening response and reach a final strength according to standard [2].

Quenching after solution annealing prevents diffusion of alloying elements, and the solid solution stays at a metastable supersaturated state, representing - together with highly-relevant quenched, i.e. non-equilibrium vacancies in Al-alloys - the prerequisite for precipitation during subsequent tempering, described in the next chapter (0). Sensitivity of quenching is increasing with an increase of either  $Mg_2Si$  or just Si. Quenching sensitivity means, that with an increase of alloying elements, the cooling rate also needs to be increased to keep the Mg- and Si-particles

in the supersaturated state and prevent their precipitation. When the cooling rate is too low, dispersoid phases represent nucleation sites for coarse Mg-Si precipitates and therefore reduces the age hardening response of the alloy [13]. If the cooling rate is beneath a critical value (680°C/min for standard AW6082 alloy in the range of 400 – 290°C), foremost equilibrium  $\beta$ -phases are built in the matrix at the cost of their precursor phase  $\beta''$ , which is mainly needed for the hardening effect. With an increase of alloying elements (Mn, Cr, Zr), cooling rates must be raised even further (up to 8000°C/min) to reach standard strength [4] [14], which would indeed be technologically extremely demanding. Tempering is conducted in the form of “natural” (-20°C to room-temperature up to 70°C, depending on alloy specification) or “artificial” (elevated temperatures) ageing, so that diffusion of precipitates can happen.

### **3.2.1 Ageing**

During the ageing process, nucleation of disordered Mg and / or Si accumulations, so-called Nano-clusters, as well as Mg-Si co-clusters form. In part, these transform into Nano-sized ordered precipitate phases with a distinct crystallographic structure as a function of increased ageing temperature and aging time. All these partial “decomposition” stages of the Al-matrix are metastable and do not occur in the thermodynamic equilibrium phase diagrams of 6xxx systems.

During natural ageing, cluster and co-cluster stages dominate within the series of metastable phases, associated with an increase of yield strength and tensile strength at the beginning of the aging process. With increasing time, these properties stay at a constant level (Figure 4). Murayama and Hono [15] also showed with transmission electron microscopic analysis that after a 70 days natural ageing time, there was no indication of precipitate particles with distinct crystal structures.

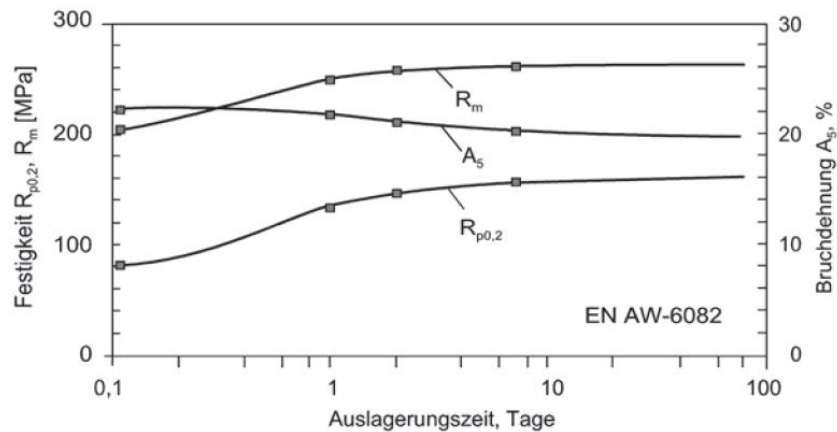


Figure 4: Change of mechanical properties for naturally aged press profiles of AW6082 alloy [4].

For many applications of 6xxx alloys, the strength obtained by natural ageing is not sufficient, and in industrial processes, artificial ageing at elevated temperatures up to 250°C is typically conducted.

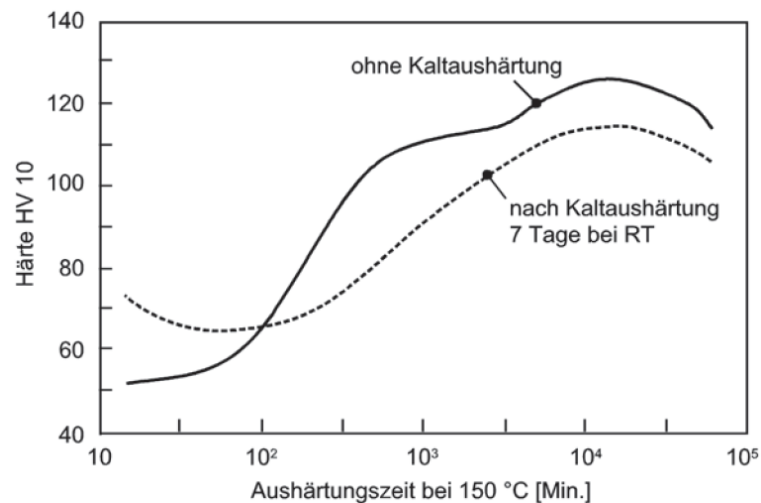


Figure 5: Trend in hardness of an artificially aged AW6082 alloy, with and without prior natural ageing [4].

In Figure 5 the curves for hardness of an artificially aged AW6082 alloy at 150°C are shown. The solid line indicates simple artificial ageing, the dashed line describes a prior natural ageing step at room temperature for 7 days. Although hardness is higher at the beginning, a temporary ageing at room temperature prior to artificial ageing delays the hardening process at usual temperatures and reduces the reachable maximum hardness [4].

The maximum hardness is achieved through fine, needle-like  $\beta''$ -precipitates with the stoichiometry  $Mg_5Si_6$ , which are (semi-) coherently connected to the  $\alpha$ -lattice.

When precipitates are connected coherently or semi-coherently to the matrix phase, a slight distortion of the lattice is achieved, which results in additional work needed for dislocations to cut through those precipitates (Friedel-effect). The goal is to achieve an ideal precipitate radius  $r_0$  that ensures a maximum increase in strength, as in simplified equation (2) in accordance with Figure 6. In the equation,  $G$  denotes the shear modulus,  $b$  the burgers vector and  $\tilde{\gamma}$  an effective interfacial energy. In Figure 6 the left and ascending line shows the impact of the Orowan mechanism, i.e. bypassing precipitates with increasing precipitate radii and the descending line characterizing the Friedel-effect. Only solid parts of both lines are significant, since dislocations will choose the way of least effort [16].

$$r_0 = \frac{G * b^2}{\tilde{\gamma}} * \sqrt[3]{3} \quad (2)$$

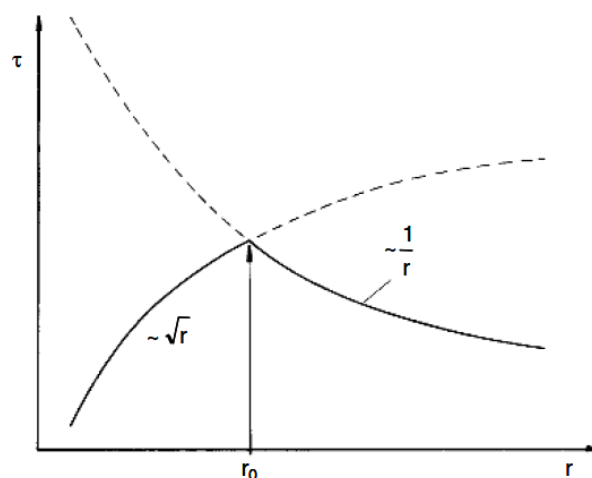


Figure 6: Relationship between strength and particle size for age-hardened alloys [16].

### 3.3 Recrystallization and coarse grain

Hot forming such as extrusion generates high deformation and strains on the raw material (also see section 5.3). Feed stock is stretched from the short ingot into a new “endless” form. As a result, the microstructure contains elongated grains in a fibrous texture. Retaining this fibrous structure and take advantage of the press effect is often desired. Press effect means, that

dislocation density and grain boundary area are increasing due to deformation during the hot working process and thereby increase strength of the extrudate in form of stored energy. Also, due to strong deformation, grains receive a preferred orientation, and therefore have orientation dependent properties (for example hardness increasing in deformation orientation, also see section 0) [17] [18]. Hot working creates a texture enriched with dislocations within the grains. This texture develops into a subgrain texture due to dynamic recovery. Recovery describes the annihilation of dislocations with opposing orientation. Recovery and recrystallization are concurring processes with the difference that recovery starts as soon as the activation energy is high enough. Nucleation and growth of recrystallized grains on the other hand are diffusion driven processes, which means aside from the stored energy within dislocations, also thermal activation and incubation time are necessary for the structure to recrystallize. The appearance of microstructure in 6xxx alloys is often characterized by dynamic recovery during hot working processes and static recrystallization afterwards [19]. Although grains are massively elongated, the subgrain texture does not show any stretching.

To receive a fibrous texture, it is essential to avoid recrystallization associated with the formation of relatively coarse grain in the material by means of adequate process parametrisation or adding dispersoid building elements to the base alloy. According to Parson et al. [18] for a fibrous core, low ram speeds (2 – 5 mm/s for ) and low extrusion ratios coupled with higher billet temperatures (depending on alloying composition) are beneficial, so that work of deformation is kept to a minimum. They showed that full recrystallization of an extruded bar cross section mainly happened at high ram speeds and low billet temperatures. However, reducing the ram speed and increasing the temperature resulted in a partially recrystallized area on the billet surface (peripheral coarse grain).

Even though AW6082 is a recrystallization resistant material, recrystallization can still happen spontaneously if the triggering parameters time, dislocation density and temperature are high enough, as described above. That's why understanding of grain growth control and thus dispersoid evolution is a strong demand for optimized product properties. Regarding parametrization, foremost heat development due to friction (see section 0) and shear stresses need to be observed. In respect of dispersoid building elements, an accurate adjustment of homogenization temperature is a critical factor (see section 0) [4]. Mn and Cr are such elements that are added to form in combination with Fe dispersoid phases during homogenization and increase the dispersoid particle distribution [13]. Hu et al. [7] claim, that the size and distribution of Mn-containing dispersoids strongly depend on the heating rate during homogenization.

According to them, the size of recrystallized grains and their nucleation rate are strongly connected to the dispersoid particle size. The benefit of dispersoids in the course of recrystallization is that they inhibit the growth of recrystallized grains and offer a resistance to grain boundary motion. By increasing the Mn and Cr concentration the volume fraction of particles is also increased and therefore the interparticle spacing is reduced. On the downside, extrusion pressure and quench sensitivity are increasing at the same time, because dispersoid particles have a strengthening effect on the structure, which reduces extrudability [20] [18].

The Zener-drag (Zener pinning) is a measure of the effectiveness of dispersoids in recrystallization resistance, which directly depends on the volume fraction and size distribution of particles after homogenization. The Zener pinning pressure, as the measure of resistance is called, is given in equation (3) [17]:

$$P_Z = \frac{3 \cdot F_V \cdot \gamma}{2 \cdot r} \quad (3)$$

In this equation,  $F_V$  denotes the volume fraction,  $\gamma$  the grain boundary specific energy and  $r$  the radius of dispersoid particles (spherical). Zener pinning bases on the principle, that when a grain boundary with specific surface energy meets a particle, a region of the boundary will be removed equal to the intersection area with the particle and so the boundary energy is reduced and the grain boundary therefore “pinned”. This effect is stronger with coherent than with incoherent particles. Homogenization (dissolving Mg-Si particles and-containing AlFeSi-phases) has an impact on size- and volume fraction of dispersoids, resulting in a reduced Zener-drag with coarser particles due to long heating times. Since it is preferable in extrusion to achieve a fibrous structure in the final product, it is essential to keep as many fine dispersoids as possible after the homogenization step.

### 3.4 Extrusion process

To successfully press material through an extrusion press, some crucial heat treatment steps before and after extrusion are necessary to achieve required mechanical properties in the end product. A typical example for temperature ranges that 6xxx Al-base material experiences throughout one production cycle is shown in Figure 7. Generally, there are two different ways for extrusion: the direct and the indirect process. Indirect extrusion means that the ram (including the die) moves into the liner and against the billet, while the billet stays still. The advantage of

this process is that there is no friction between billet and container, which means that extrusion force is entirely used for plastic deformation and that temperature profile, and thus microstructure, is more uniform [4]. Since the laboratory press used in this thesis works on direct extrusion principle, this will be the focus and explained exclusively henceforth, see chapter 3.4.5.

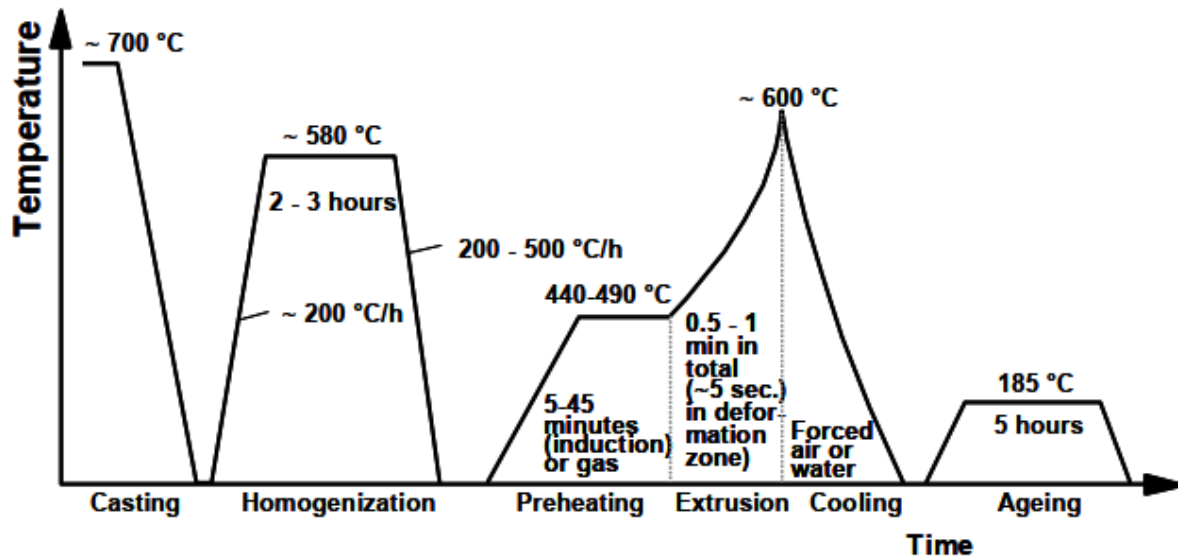


Figure 7: Temperature-time regime for whole extrusion process [12].

### 3.4.1 Casting

The first step in manufacturing of aluminium profiles is the production of ingots. The most common process for producing billets is direct chill casting (DC-casting). Therefore, a combination of virgin aluminium, scrap and alloying elements are mixed together in a furnace and heated up to temperatures of about 700°C. For adequate ingot quality, thorough mixing of components, effective fluxing, degassing and filtering of the melt before casting are essential. These treatments remove dross, oxides or other non-metallic impurities from the melt. Hydrogen shows a distinct solubility in the aluminium melt and is rejected from solution during solidification, converging to molecular hydrogen gas. This gas is then trapped in the solid structure and leads to higher porosity of the cast material. Thus, provisions are to keep hydrogen content in liquid metal beneath 0,15 cm<sup>3</sup> per 100 g and to purge the melt from hydrogen. This can be done by bubbling an insoluble gas through the melt or continuous fumeless in-line degassing [1] [21].

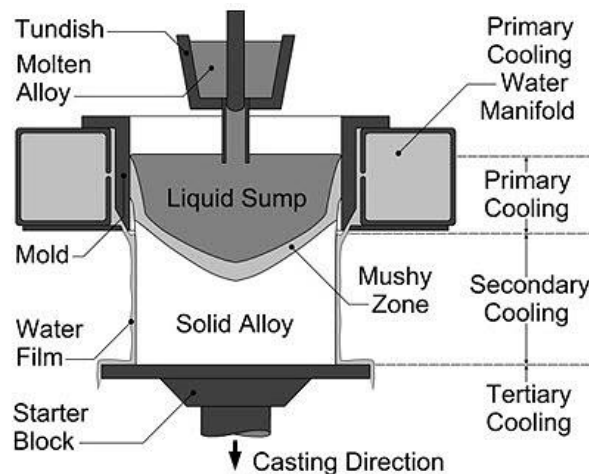


Figure 8: Vertical DC-casting scheme [22].

DC-casting is a semi-continuous method that produces a uniform ingot structure. The vertical process as shown in Figure 8. is preferred to the horizontal DC-casting, because microstructure (mainly grain size and unsymmetrical formation of segregation) is more difficult to control in the latter one. Generally it can be said, that the horizontal process is better suited for casting of small, continuous cross sections, whereas the vertical casting is used for bars with diameters of 90 mm upwards [1] [23]. The melt is poured into one or plural water-cooled moulds that have retractable bases. Solidification is then reached in two steps: in the primary cooling step the metal solidifies at the circumference of cooled mould wall. The bottom block is slowly being lowered then. The remaining inner section is solidified through sub-mould spray cooling. In this secondary cooling step, the semi-solid shell that leaves the bottom of the mould is directly impinged with cold water that runs down at the surface of the ingot. This water spray contact is responsible for the major part of heat extraction. The casting hence continues until the desired ingot length is reached.

Problems that might appear are a rippled cast surface due to stick-slip contact of melt with mould wall, resulting in surface tears or microstructural inhomogeneities. Therefore, it can become necessary to machine or scalp DC ingots prior to extrusion [1].

### 3.4.2 Homogenization

Homogenization procedures give the advantage of an improved extrudability, superior surface quality and higher strength of the extrudate end product [6].

The main objectives of this heat treatment are: firstly, reducing the effects of microsegregation, secondly removal of non-equilibrium eutectic phases, because of their low melting point and the resulting risk of cracking during subsequent working processes and thirdly a controlled and homogenous precipitation of elements that were dissolved during solidification step [1]. In the context of phase transformations, the commonly known  $\beta$ -to- $\alpha$  transformation is significant for the extrusion process. In this transformation the plate-like  $\beta$ -AlFeSi convert to more globular cubic  $\alpha$ -Al(FeMn)Si. During extrusion, brittle  $\beta$ -particles might cause surface defects due to local crack initiation, whereas the  $\alpha$ -particles improve surface quality and extrudability because of their more ductile behaviour. Since dissolution of  $Mg_2Si$  particles is rather fast compared to the  $\beta$ -to- $\alpha$  transformation, the latter define the required homogenization time. The transformation rate is influenced by many parameters, such as homogenization temperature, as-cast microstructure and alloying elements. Out of the alloying elements in 6xxx alloys, Mn has the biggest influence on  $\alpha$ -phase stability and transformation rate, whereas an increase of Si decreases speed of transformation [24].

(Partial) incorporation of, e.g., Mg and Si in dispersoids in the scope of homogenization is further important for optimised extrusion, since Mg and Si in complete solution increase the flow stress of the alloy, increasing the needed press energy because of additional resistance of deformation.

A high quenching rate keeps Mg and Si in this entirely dissolved supersaturated state, whereas a rather slow cooling rate promotes formation of equilibrium  $\beta$ - and  $\beta'$ -phases (see section 3.2) The latter is also unwanted because of the risk of incipient melting of those  $\beta$ -phases during extrusion and the absence of  $\beta''$  precipitates for the age hardening. It is desired to apply a cooling rate, that brings enough Mg- and Si-particles in solution, which will precipitate in a way, that they survive the extrusion pre-heating and dissolve right before exiting the extrusion press, to ensure maximum hardening during the subsequent ageing [6].

Annihilation of microsegregation is mainly reached through diffusion of alloying elements from high element concentrations to low ones, i.e. from (due to non-equilibrium microsegregation) enriched to depleted regions, often from grain boundaries inwards, or from interdendritic regions to dendrite cores. Time for this process is determined by diffusion distances due to grain size or dendrite arm spacing and rate of diffusion of the alloying elements. Since diffusion is a temperature driven process, an increase in temperature shortens the time for homogenization and vice versa. Technological homogenization times usually vary from 6 to 24 hours (including heating up, dwell and cooling down).

Homogenization of ingots for the extruding step normally takes place in a temperature range of 450 – 600°C (depending on specific alloying composition) [25]. It is of importance though, to keep homogenization temperature low enough to prevent incipient melting of eutectic or low melting phases, which would cause permanent microstructural damage [26]. This can be controlled by using thermodynamic equilibrium computations, evaluating the thermodynamic stabilities of eutectic phases.

### **3.4.3 Pre-heating**

Pre-heating is an important step for the extrusion process, because the higher temperatures facilitate flowing of material and therefore reduce the needed compressive forces [4]. Usually pre-heating of billets is ensured with either an induction furnace or a gas-fired furnace or a combination of both. The requirements to an oven are to be quickly ready for operation, full-automatic operation, exact temperature control on every billet, uniform heating, short heating times and a fast and easy adaption to changes in material or extrusion press temperature conditions. Generally it can be said, that due to heating mechanism gas-fired furnaces take 3 – 4 times the time for heating compared to induction ovens [27].

Pre-heating temperature normally varies for aluminium alloys in a range of 450 – 500°C [4]. If taper heating is needed (see section 0), the front end directing towards the die might be heated up to a 100°C higher temperature than the tail end [27]. The time needed to completely heat up the billet to the desired temperature strongly depends on the billet size.

### **3.4.4 Extrusion**

#### **3.4.4.1 Overview**

The pre-heated billet is transferred to the extrusion machine and thereafter pressed. The extrusion process is executed in approximately 1 minute, depending on the size of the billet and process parameters. In case of the laboratory press, with high ram speed and a small billet size, the pressing took about 5 seconds. As Figure 7 indicates, during the extrusion process, heat is increasing significantly, as described in detail in section 0.

#### **3.4.4.2 Parts of extrusion plant**

Extruding of aluminium alloys can be achieved in a direct or indirect process, hot or cold, depending on the alloy. In this context, only the hot extrusion will be discussed. As for direct or indirect extrusion, the direct process is the more common method, due to great versatility in extrudates' dimensions whereas at indirect extrusion, the size of the cross-section is confined

by the stem size. Since the laboratory extrusion press of this thesis works on direct principle as well, focus will only be put on the mechanisms of direct extruding. The key factor to distinguish these two systems, is that in direct extrusion the metal flow is in the same direction as the ram travel, whereas at indirect extrusion, the billet material does not flow and only the ram is moving, which has the advantage of avoiding friction between container wall and billet [26].

The main parts of a press are shown in Figure 9. The container of a press is definitely one special part, since it is quite expensive and its lifespan often defines the profitability of an extrusion plant. For best performance of the press, it is important that container with liner, stem with dummy pad and die slide with die stack show proper alignment [26].

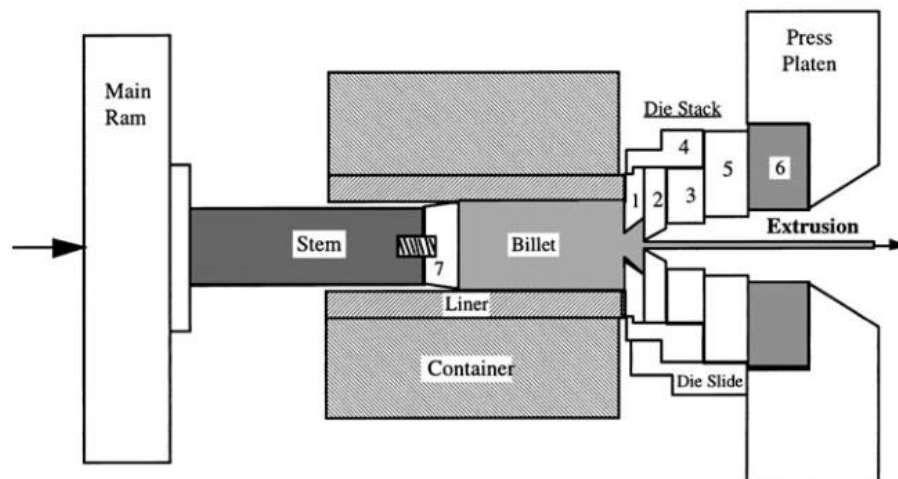


**Figure 9: Configuration of a direct extrusion press: 1...feeder plate, 2...die, 3...backer, 4...die ring, 5...bolster, 6...pressure pad, 7...dummy block [26].**

The main ram moves hydraulically and transfers the generated force on the stem and dummy pad. Dummy blocks can either be fixed (industrial standard) or variable. In the case of the laboratory press, the dummy block was threaded and therefore easily mounted on the stem [26].

The principle of a feeder plate is to put a welding chamber in front of the die opening and therefore ensure an even flow of material through the die hole. The feeders opening itself is smaller than the billet circumference and opens then, so that metal can flow with equivalent speed through the actual die. For the laboratory press there was no feeder used, but a die-integrated recess opening instead. Compared to the feeder plate, the shape of the cavity for recess dies is converging, so metal is flowing faster through the die hole, due to volume consistency [26].

The die realizes the actual geometry of the extrudate. The layout of the die depends on the product that should be realized with it. Possible shapes are solid shapes (bars, rods), hollow shapes (tubes) or even more complex profiles (semi hollow shapes). For a solid shape, a solid single hole die might be sufficient. For more complex or hollow profiles, a multipart-die with an orifice-mandrel system is needed. Dies are built as single-hole or in multi-hole form if possible, to increase output in industrial plants. Thickness of the die was reduced over the years, as compressive forces are mainly absorbed by the whole die stack, namely by backer, bolster and pressure pad [28]. However, there are multiple die backing design strategies. Though the overall strategy for all supporting tools is to minimize the die deformation and deformation of the extruded product. The interfaces of support tools should generally be as tight as possible. On the other hand, in industrial facilities change of parts must be easy to carry out because charges are often small and tools worn out or broken [29].

#### *3.4.4.3 Feeding – influences and mechanical properties*

Although the process is at its core not continuous, it is possible to produce continuous lengths of a given geometry by performing billet-on-billet extrusion. In that case, billets are consecutively fed to the extruder and are welded together just within the container. Essential conditions are good weldability of the material at the temperature of deformation, cleaned billet surfaces and ends freed from grease, and air exclusion to avoid blisters and other defects. The discard of the first billet could either be removed or just be pressed onto with the second billet [26].

The outside billet diameter is a little bit smaller than the container bore hole, so that it can easily be fed. The material behaviour is thermoplastic-viscoelastic. It expands a little due to heating but is also compressed elastically [29]. The ram pushes the billet forward until it has contact to the die stack surface. Then the billet is extended in diameter until it is in full contact with container walls, which leads to an increase in extrusion force. From this point on material is starting to flow through the die hole. The material starts to flow, when the stress exceeds material flow stress. Flowing aluminium mainly undergoes shear stresses, because the centre of the billet is flowing faster than the periphery [26]. Because of the sticking friction and retardation of material at the periphery, strain rates at the outlet of the die may be locally extremely high (up to  $10000 \text{ s}^{-1}$ ). It only flows towards the billet centre when the ram comes close to the die (Figure 10(a)). This has the benefit, that oxides and other impurities accumulate in the rear billet section and can then easily be cut off [29]. The breakthrough point marks the spot of maximum extrusion pressure (Figure 10(b)). Pressure is then decreasing continuously with ram displacement since surface-friction between billet and wall is also decreasing. Just in the end, when the remaining material

in the dead metal zone needs to flow radially, the load is increasing again and the billet butt is pressed through the die hole.

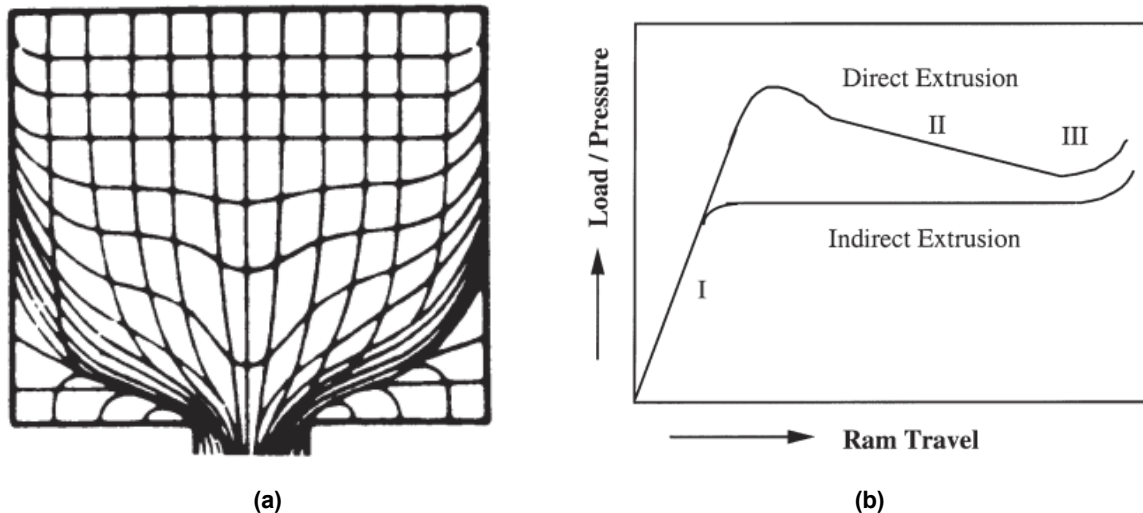


Figure 10: (a) Schematic of flowing material during extrusion. (b) Pressure profile of direct and indirect extrusion changing with ram displacement [26].

#### 3.4.4.4 Temperature development

Heat development during the extrusion process is one of the key factors for overall product quality, as well as dimensional stability, extrusion defects and mechanical properties. It is also important for the lifespan of extrusion equipment, especially the die wear and the die performance. The critical temperature is the exit temperature, when the metal leaves the die. Heat conduction normally requires a certain amount of time. For high ram speeds, heat generation outweighs heat losses in the process. The following factors mostly influence the billet temperature profile [26]:

**Material properties:** Mechanical as well as thermal properties are of great importance. On the thermal side, it is mainly heat conduction that increases temperature. On the material side, mostly deformation work and friction generate a temperature rise. Dissipated heat is proportional to the flow stress of the material at a given temperature, strain and strain rate. In case of friction, generated heat is proportional to the friction shear stress.

**Friction:** Heat generation depends essentially from the friction factors of billet and container interface, material and die interface and the friction shear stress at the dead metal zone interface.

Ram speed: The extent of generated heat is affected by the strain rate. So, temperature in turn increases with increasing ram speed, because it is directly proportional to the strain rate. Besides, the lower the ram speed, the more time for heat to be conducted either to the surrounding components or to the extrudate centre, especially with aluminium alloys, since thermal conductivity is quite good.

Extrusion ratio: The higher the extrusion ratio, the more plastic deformation is performed and thus strain also increases.

Outside perimeter: Temperature increases with increasing outside perimeter of the extrudate, because this is intrinsically tied to an increase of die bearing area, due to larger perimeter of the die.

The ideal process is isothermal extrusion, i.e. pressing with constant exit temperature of the extrudate. The benefits of this process management would be improved dimensional stability, a uniform surface quality, consistent mechanical properties with a uniform microstructure, faster extrusion speed to increase productivity and reduced breakthrough pressure. To perform extrusion isothermal, it is first necessary to gain knowledge of the relationship between ram speed and exit temperature for the given process variables. Therefore, it often is the easiest way to determine the temperature characteristics at constant ram speed and then check feasibility of isothermal extrusion by means of press control system. Usually, the exit temperature is continually increasing. To gain an isothermal exit temperature profile, there are mainly two ways that are industrially common (see also Figure 11) [26]:

1. Reducing the exit speed while extruding according to an on-line noncontact continuous temperature measurement. The control cycle then regulates the ram speed according to live measurements.
2. Taper heating or taper quenching the billet. In this case, billets are either pre-heated in different temperature zones or uniformly heated and then cooled down right before entering the container. The aim is to produce a temperature gradient on billet axis, transferring more heat to the front than to the rear. Attention must be paid that the process is not delayed at any time, because good thermal conductivity of aluminium would cause the temperature gradient to vanish.

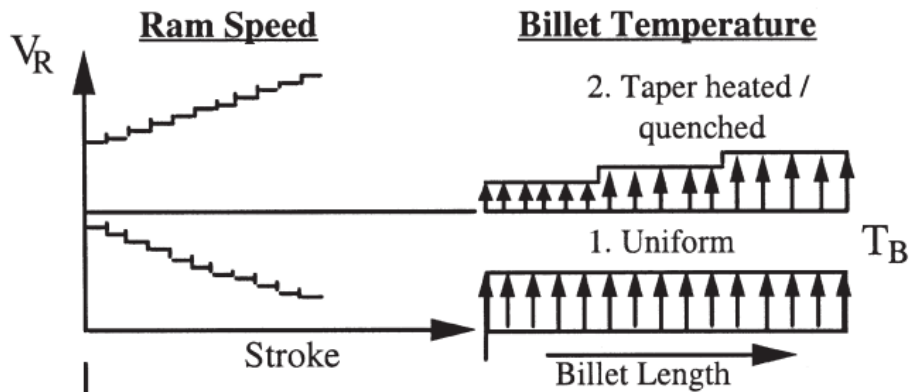


Figure 11: Principle of taper heating or variable ram speed for isothermal extrusion [26].

In production environment, a combination of taper heating / cooling and variable ram speed is seen to be most efficient. Pre-heating the billet axial to different temperature zones and then feeding it to the container with variable ram speed enables Isothermal extrusion [26].

Quenching of the extrudate can be achieved either using air fans, a water tank (cold water, tempered water or oil), or more commonly, a water spray system. The critical temperature range when quenching lies between 400 and 290°C. It is of importance, to quickly pass this temperature range to avoid unwanted decomposition of the supersaturated matrix state or, in other words, nucleation of new  $\beta$ -phase and its precursors (also see section 3.2). Cooling rates depend on material dimension, profile dimension and medium for quenching. The goal is to quench as quickly as needed, to meet the desired strength requirements, but at the same time to avoid distortion of the end product. Because of stresses during quenching, but also from extrusion, it is necessary to stretch the extrudate, followed by cutting it into the right dimensions before continuing with either another forming step (such as bending) or the ageing step for maximising strength. Cold work hardening of Al-Mg-Si-profiles increases strength of material a little but at the same time reduces ductility. Slight plastic deformation during straightening (<2%) showed a negligible effect on ageing performance though [4]. Precipitates that originate during homogenization should, at optimum, survive the subsequent pre-heating to maintain extrudability, but dissolve during extrusion to ensure maximum hardness when being aged. This

is especially important, if the product is treated as a T5<sup>2</sup> temper without an additional annealing step.

#### 3.4.4.5 Friction during extrusion

For direct extrusion, the main friction components are shown in Figure 12. As can be seen, in the corners of the die face and the container wall a dead-metal zone of material is built. Compared to flowing material in the middle, material at the border to the conical dead-metal zone undergoes shear deformation. Hence, the friction between dead-metal zone and flowing material equals the shear stress. The dead-metal zone semiangle  $\alpha$  is a function of extrusion ratio (ER), flow stress ( $\bar{\sigma}$ ), friction factor ( $m$ ) between billet and container interface and the friction factor of flowing metal and die bearing interface ( $m'$ ) and has an input on product quality and butt thickness, hence profitability of the process. Therefore, it is necessary to stop the process at a safe margin zone, to avoid getting oxides and other inclusions into the product [26].

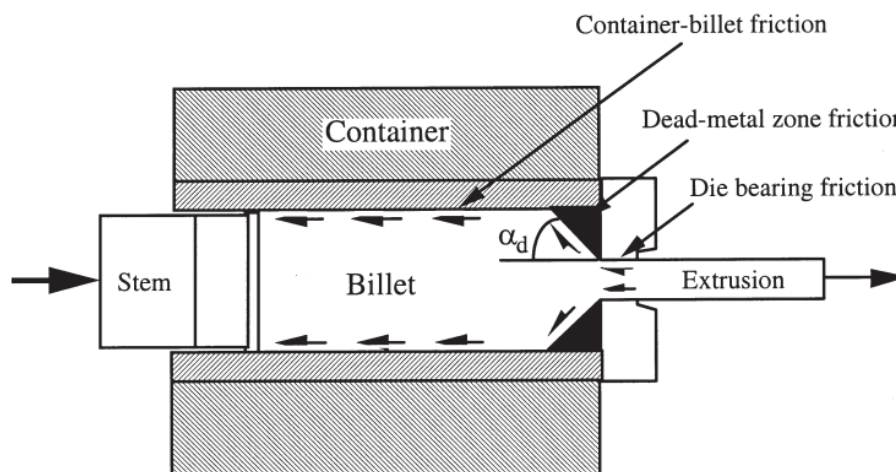


Figure 12: Friction components in direct extrusion plants [26].

Friction at the interface of billet and container could be considered in two conditions: either it is sticking friction or sliding friction, which means a lubricated interface flow is ensured. Since pressure during extrusion is high, resulting in an even larger area of contact, the friction is considered to be sticking. This results in skin of billet surface being separated of the body and sticking to the container wall [26].

<sup>2</sup> T5...Cooled down from elevated temperature after forming followed by artificial ageing

As for the die bearing friction, it is assumed that because of adhesion from aluminium with die material, a thin layer is built, that progressively grows with press cycles until the die bearing is totally covered. As soon as the die bearing is covered with an aluminium layer, a change from sliding to sticking friction is happening. To avoid this procedure as well as to reduce tooling costs, die surfaces are hardness coated or nitrided to increase wear resistance. Nitriding was also performed on all dies that were used for this thesis, about halfway through experimental time. Then again, friction of die bearings is also used to balance differences in material flow through the die. The bearings control size, shape, finish and speed of extrusion. Since container friction retards the billet surface, the centre of the billet material is flowing faster. This surplus of flowing metal can be balanced through a longer bearing length in the centre of the die, whereas at the die rim, the bearing length should be shortened to compensate the metal flow. It is important to avoid sharp changes in bearing length though, because an uneven flow might cause streaks in end product [26].

#### **3.4.5 Artificial Ageing**

Artificial aging with acceptable furnace time can be conducted in the range of 160 – 185°C for 5 – 8 hours for most of the aluminium alloys.[4]. Often the time-temperature regime is adapted to a convenient duration, such as 8 or 16 hours going along an industrial shift. Attention should be paid to the risk of overageing the alloy during artificial ageing though, which will reduce the maximum hardenability. Compared to natural ageing, hardness first increases depending on the alloy up to a certain maximum and then decreases again. Maximum hardness can generally be achieved for a given temperature, with a decrease of ageing temperature and an inverse prolonging of ageing time, going along with highest driving force for  $\beta''$  nucleation but slow kinetics, decelerated growth and impeded transformation to overageing phases. However, this maximization in hardness is at the expense of process time. For industrial application, a reasonable (and delicate) agreement between these two parameters is to be made.

Time between extrusion process and artificial ageing should be kept as short as possible (maximum 1 – 2 days) or, if necessary, be bypassed with a stabilisation annealing at approximately 80°C. This is of importance, because during unwanted downtime after extrusion, material undergoes natural ageing going along with the formation of early precipitation of cluster stages. This cluster formation is reducing the final strength that can be reached during a subsequent artificial ageing treatment [28]. Even though the precise mechanisms for this effect are still not fully understood and a matter of ongoing scientific debates.

## 4 Experimental

### 4.1 Extrusion press and handling

#### 4.1.1 Furnace setup

The furnace used for pre-heating was a model *Carbolite CWF 1300* with an integrated PID control unit *Eurotherm 3216*. The main goal was to find a setup for the furnace that reduces pre-heating time to a minimum while assuring that billets are heated to the desired temperature. Reducing pre-heating time is on the one hand interesting for increasing time efficiency (mainly for industrial applications), on the other hand optimisation of pre-heating to increase extrudability and quality of the end product is desired. Therefore, it was necessary to gain knowledge of the temperature gradient on the billet cross section. This could be achieved by positioning type K thermocouples on billet surface and core. The thermocouples were connected to a *Multichannel Recorder MCR-4 TC* data logger to record and visualize measurements. For the first test series (AH1 – AH5) two extruded billets (see Billet 1 and Billet 2 in Figure 13(a)) were used. For second test series (AH 6 – AH10) two cast billets (Figure 13(b)) of material AW6082 were used. Core temperature measurement in series AH1 – AH5 was conducted via two holes that were drilled to mount thermocouples, one in radial direction in mid billet height, the other one in axial position at the cross-sectional centre. Due to contact errors of the thermocouple in axial position only data from the one measuring core temperature in radial position could be used though, which is also the reason why the axial position is not shown in Figure 13a. The fixation of the core thermocouple in billet 1 was carried out with a temperature conductive two component ceramic paste. The thermocouple for surface measuring was pinched in a small surface crack of billet 2. For the series AH6 – AH10 the axial thermocouple was also jammed in the bore, by slightly deforming the top surface of the billet with a centre punch. The exact dimensions and positions of the thermocouples used for measurement are all shown in Figure 13.

For pre-heating billets to 420 / 480 / 540°C core temperature, the oven was set at 600°C and heating conducted for 26 / 30 / 50 minutes. The results to achieve these parameters are described in section 5.1.

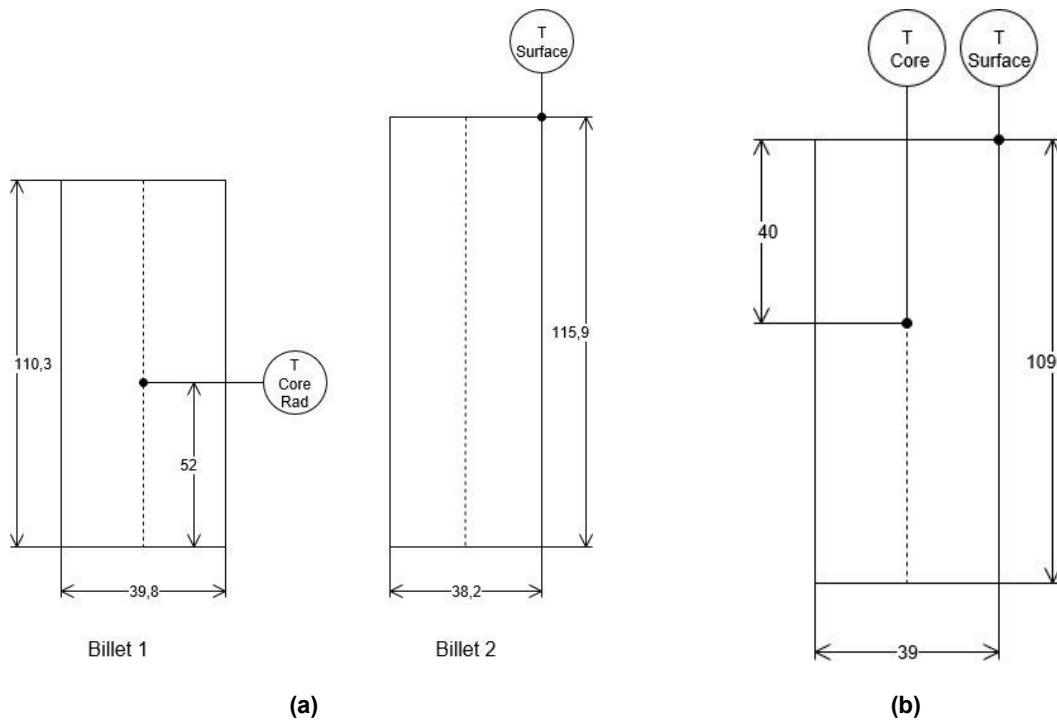


Figure 13: Dimensions of billets and thermocouple positions for (a) AH1 – AH5 and (b) AH6 - AH10.

#### 4.1.2 Furnace – press transition

Transfer of pre-heated billets from the furnace into the also pre-heated extrusion press container was carried out manually. In Figure 14 cooling rates for four different measuring points are shown. Billets were taken out of the oven at around 450°C and cooling rates were measured for the first three minutes. Linear regression showed, that material is cooling with a rate of approximately 18°C/min or 0,3°C/s. With a time period of about 20 seconds from getting the billet out of the oven and putting it into the container, this means a billet “loses” 6°C during transfer. This decrease of temperature was considered, by slightly overdoing the pre-heating time in the furnace.

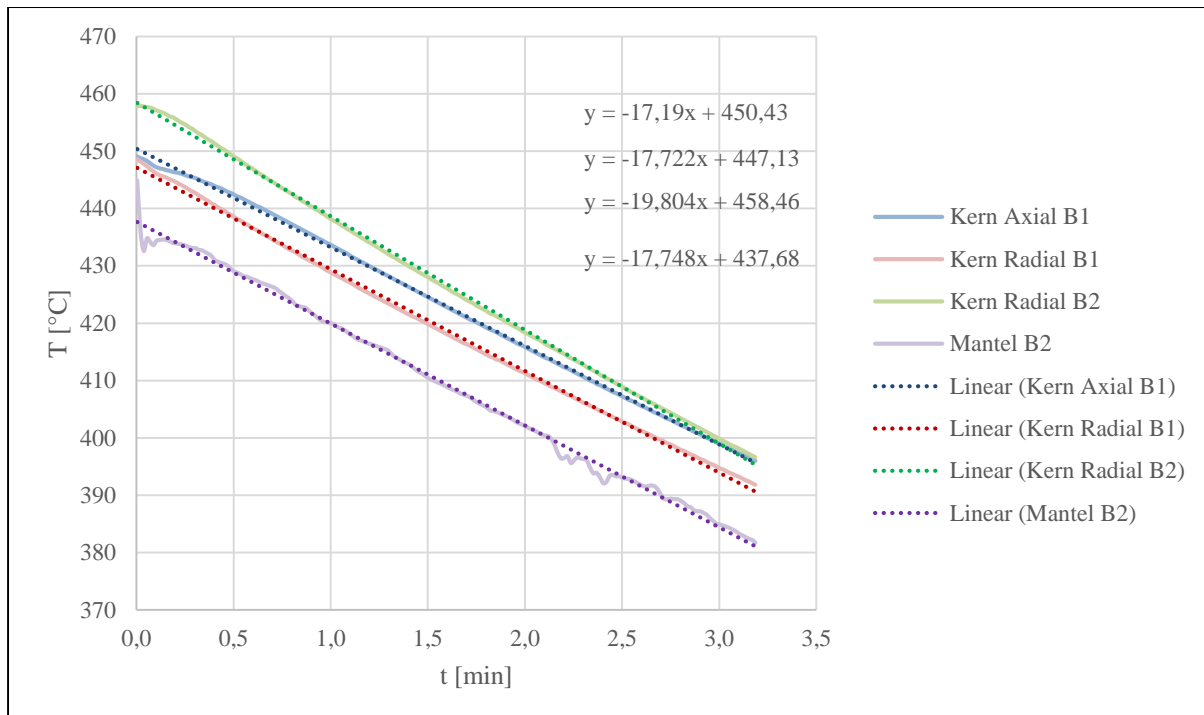


Figure 14: Cooling rates for billets from 450°C at ambient conditions with regression lines and corresponding equations.

#### 4.1.3 Extrusion press and cooling

The laboratory extrusion press, whose parameters should be optimised in the course of this work is shown in Figure 15. The main cylinder measures 30 cm in diameter and is able to press with a force of up to 2 MN. The container temperature was set to 350°C via an extern PID controller. The temperature of the container and liner was not changed throughout the whole experiment, because it has negligible impact on mechanical properties of the extrudate. It has an influence on the surface quality of the end product though. Main functions of the container are to maintain the bore cylindrically stable and to obtain a constant temperature distribution throughout the axial direction. On one hand, the container needs to be heated, so that the hot-working steel (1.2343) that is used as construction material achieves the needed ductility to ensure crack-free operation of the liner. On the other hand, too high temperatures in liner or mantle can lead to a loss of strength and therefore cause permanent deformation and malfunction. While the liner is a wearing object of utility and can be replaced in a regular interval, the container mantle has in industrial applications a life span of up to 15 years. Furthermore, axial temperature gradients during extrusion process must be considered. A permanent and excessive temperature increase on the tool side could cause for example blisters on the aluminium profile or burn marks in the liner bore. These burn marks originate from air inclusions

that lead to incipient melting and may cause an axial crack and, as a consequence, failure of the press [30].

The installed press controller enables the user to operate three different functions: firstly, movement of the container, to ensure a tight transition from liner to die stack. Secondly the die stack, for the purpose of die change as well as shearing off butt material from extruded product and thirdly the ram, with a control dial scaled 1 to 10 to regulate ram speed. The control dial was malfunctioning though, which resulted in a non-adjustable ram speed of 47 mm/s. Ram speeds are usually in a range from 5 – 11 mm/s for the 6xxx alloys, depending on many factors, such as extrusion temperature, pressure, ER, metal flow through die or surface defects [26], [31]. However, studies and simulations have been conducted with ram speeds of up to 30 mm/s [18].



**Figure 15: Laboratory extrusion press.**

In the current state, when experiments for this thesis were conducted, there was no rack for either directing nor for cooling the extruded products. Therefore, extrudates of all forms basically bent down after extrusion and fell to the ground after being cut off through die stack movement to the outside. After pressing one billet, the container was disposed of material leftovers by pressing a cleaning disc through the container hole. Leftovers of the billet butt, which remained in the die after the extrudate was sheared off, were cut out manually. At the end of each pressing session, with a maximum of 11 billets that were pressed during one session, all used die-geometries as well as the cleaning disc were immersed in NaOH-base for dissolving alloy leftovers from their bodies.

Cooling for the standard routine was conducted through air at ambient temperature, i.e. a relatively slow mean cooling rate of 5°C/min in the range of 500 – 50°C. For achieving different temper states of extrudates (T5, T6), the cooled-down material was cut to pieces of 2 cm length, followed by a heat treatment in the same oven as described in section 0. Quenching for the T6 temper was executed by manually putting the specimens into a bucket filled with tap water, so cooling rates for this step could not be quantified.

## 4.2 Die geometries

One goal of this thesis was to test if all die geometries for this press would work. For simplification, the different die shapes shall be abbreviated as shown in Table 3:

**Table 3: Denomination and dimensions of all used die geometries.**

Abbreviation	Form	Dimension [mm]
<b>RW</b>	Rectangular bar	4 x 20
<b>W10</b>	Rod, 1-hole die	Ø10,5
<b>W5</b>	Rod, 2-hole die	Ø5
<b>QW</b>	Square bar	10 x 10

Images of all dies are also shown in Figure 16(a) – (d).



(a)



(b)



**Figure 16: Used die geometries: (a) RW-die, (b) W10-die, (c) W5-die and (d) QW-die.**

Because of this test series, maximum pre-heating temperature for this extrusion press turned out to be 540°C. At this billet temperature material already seemed to be so soft, that the extrusion process chocked in the cavity at die end, resulting in random extrusion forms, as shown in Figure 17(a) and (b).

On the other hand, first press series with low billet temperature (around 300°C) material showed especially for the W5-die with high deformation considerable resistance to flowing, resulting in a faulty extrudate, where only one string exited the two-hole die. This probably happened, because of minimal differences in friction between the two-hole die bearings. When temperature was too low, at the same time flow stress of the material was too high, so all material exited through the hole with less resistance. With an adequate billet pre-heating temperature of 480°C extruding through all four dies was easily achieved.

Block-on-block pressing was also tested, with and without pre-heating of the die. This procedure was not executable without pre-heating of the die, because of the extrudate's butt, plugging the die after one pressing sequence. When pre-heating the die alongside with the billets, block-on-block extruding was successful.

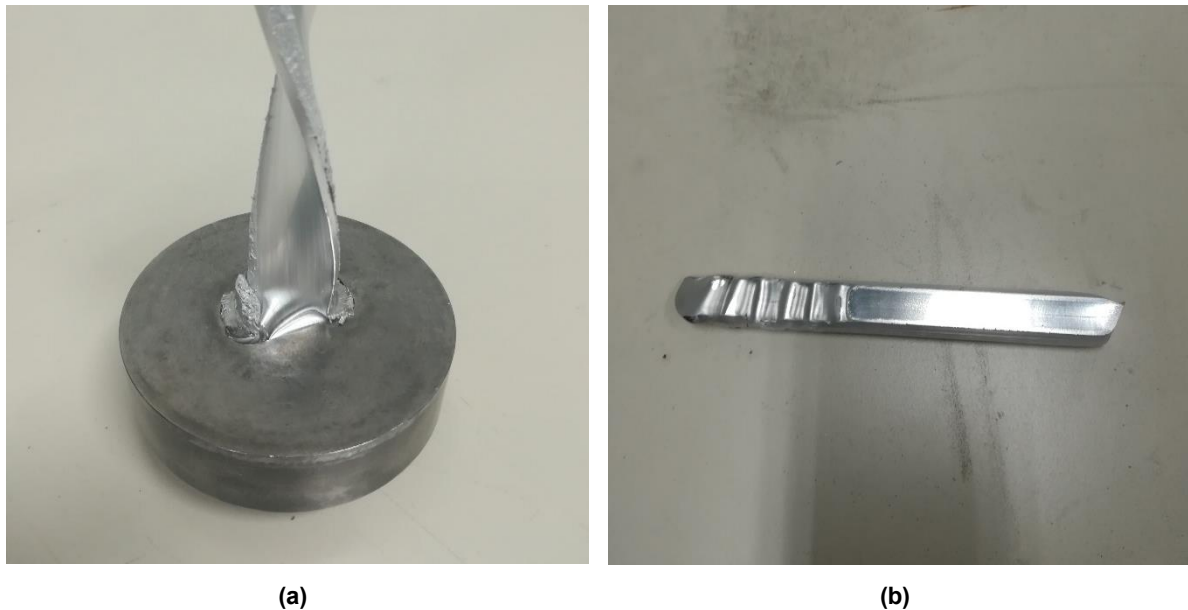


**Figure 17: Deformations of extruded products because of too high pre-heating temperature: (a) plugged RW-die with twisted extrudate and (b) rectangular extrudate distorted and out of dimension.**

### 4.3 Thermal routes

Impact of different pre-heating temperatures on mechanical properties of the end product, as well as several thermal routes after extrusion were tested by means of hardness testing. An overview of tested geometries and thermal routes is given in Table 4. The notation of thermal routes is in accordance with standard DIN EN 515:2017 [32]. Furthermore, the T6 alloy was actually tempered in four different ways: The specimens were solution annealed for 5 minutes and 30 minutes respectively (including pre-heating time). After quenching, each of these two metastable states were artificially aged for either 0 or 5 hours. Quenching was performed with water at room temperature. Solution heat treatment was performed at 560°C, artificial ageing at 180°C respectively. Computed thermodynamic equilibrium phase fractions as function of temperature for the chosen AW6082 specification with *MatCalc* indicated a dissolution of Mg<sub>2</sub>Si-phases at 570°C (see section 0). With that in mind, the assumption was met, that after a short time period enough Mg-Si particles might be in solution to show a hardening response after quenching. This should indicate if temperature and time during extrusion might also be sufficient to show this hardening effect. For that reason, one-time interval for solution annealing was chosen to be 5 minutes (including pre-heating).

Table 4: Overview to tested pre-heating temperatures and thermal routes.

	T1	T5 (3h)	T5 (6h)	T6 (5min)	T6 (30min)
<b>QW<sub>480°C</sub></b>	✓	✓	✓	✓	✓
<b>RW<sub>420°C</sub></b>	✓	✓	✓	-	-
<b>RW<sub>480°C</sub></b>	✓	✓	✓	-	-
<b>RW<sub>540°C</sub></b>	✓	✓	✓	-	-

Outcome of these different thermal routes is described in section 5.5.

#### 4.4 Analyses of microstructure

One main technological interest associated to this thesis concerns the obtained grain size and grain distribution variations as function of extrusion parameters for different dies. The method chosen for analysing microstructure was light optical microscopy (LOM). The used microscope was a *Zeiss Axio Imager.M2m* with a mounted *AxioCam MRc5* camera for photomicrographs. Prior to examination, specimens were evened out on a plate with modelling clay to ensure a maximum of sharpness in the observed area. Magnifications were varied in a range of 12,5 to 500 times. The Specimens were analysed in the short transverse (ST) plane for determination of grain size and in the short longitudinal plane (SL) to investigate stretching of grains.

As a reference material, the homogenized probes were analysed as well as the hot formed ones in the as-extruded state and in subsequent tempered states. All specimens were cut to a length of approximately 1 cm, long enough to stick out on the backside of the embedding compound so that best possible current conduction for Barker's etching is ensured. The specimens were cold embedded in a two components composition, consisting of electrically conductive powder and a hardening agent in a volume-ratio of 2:1. Examples of embedded specimens are shown in Figure 18. Specimens on the bottom left (RW-die) and middle (QW-die) show the ST-plane, specimens on the top left and middle the LT-plane respectively.

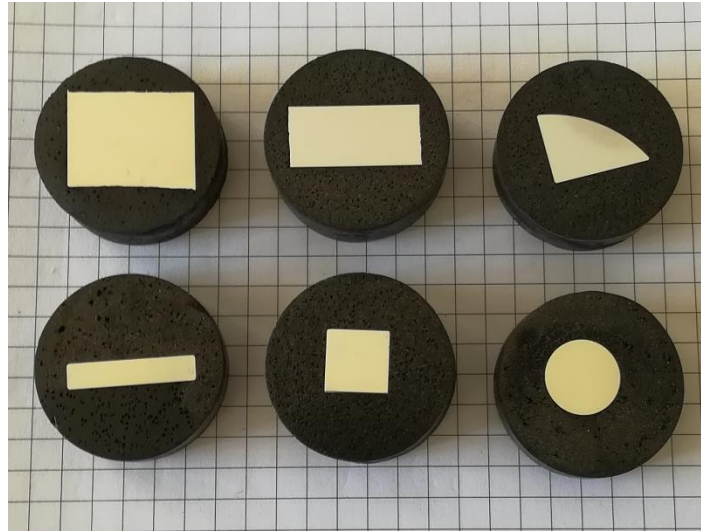


Figure 18: Embedded specimens for the RW-die (Left), the QW-die (middle), the W10-die (bottom right) and in not-extruded homogenized condition (top right).

Afterwards, mechanical grinding and polishing of specimens was conducted, using a *Struers TegraPol-31* apparatus. The parameters used for every grinding and polishing step are shown in Table 5. Between each preparation step, all specimens and their holder were washed with cold water followed an immersion in an ultrasonic cleaning device to get rid of abrasive leftovers from the previous preparation step. The direction of rotation was synced for the grinding and polishing disc for all preparation steps. The force given in Table 5 is the applied force on each specimen, meaning the force on the specimen holder is 6 times bigger. After the last polishing step (OP-U) specimens were also washed with pure ethanol, fan dried and, if not etched right away, stored in an exsiccator filled with silica gel ( $\text{SiO}_2$ ) to avoid formation of a thin oxide layer ( $\text{Al}_2\text{O}_3$ ) on the polished aluminium surface due to air humidity.

Table 5: Parameters for grinding and polishing with preparation machine *TegraPol-31*.

Step	Force [N]	Grit / Grain	Time [min]	Upm [ $\text{min}^{-1}$ ]	Lubricant	Abrasive	Force [N]	Treatment
SiC-paper	15	#320	2	300	Water	-	15	Grinding
MD-Largo	20	9 $\mu\text{m}$	5	300	Blue	DP-P	20	Diamond polishing
MD-Dac	15	3 $\mu\text{m}$	4	150	Red	DP-P	15	Diamond polishing

<b>MD- Chem</b>	10	-	1,5	150	-	OP-U	10	Oxide polishing
---------------------	----	---	-----	-----	---	------	----	--------------------

### Etching:

To determine grain size in the centre of extrusion cross section with a fine and fibrous structure by the means of LOM, several etching methods, such as Graff and Sargents, Keller or Weck's etching were tested. All of them led to none-satisfactory results, since magnification and resolution with LOM was not sufficient for the purpose of determining grain size according to standards [33] [34].

For subsequent analyses, specimens were mainly etched using electrolytic etching after Barker. One electrolyte was used several times and stored in a refrigerator in between extrusion sessions. Barker etching was performed with a rectangular 2 cm<sup>2</sup> cut-out mask at a flowrate of 20, with voltage of 25 V for 60 seconds. Following the etching, specimens were immediately washed with tap water, then pure ethanol and finally fan dried. LOM analyses was executed right away, using polarized light.

Another etching method that was used to represent dispersoids as shown in section 5.6 was a solution of 0,5% HF in water. Therefore, specimens were immersion etched in a mixture of 79 ml deionized water and 0,7 ml HF, for 35 seconds at room temperature. Cleaning and drying after the etching was conducted the same way as for Barker's etching. LOM was this time executed using bright field microscopy.

## **4.5 Hardness testing**

Brinell hardness was chosen as test method for comparison between material conditions. The measurements were executed by means of the testing machine *Emco Test M1C 010*. As an indenter, a ball sphere made of tungsten carbide was used. This is indicated by the suffix *W* in the hardness unity.

The ball indenter (*D*) was of diameter 1 mm, the applied load factor was 10 according to EN ISO 6506-1 [35], which leads to an applied force (*F*) of 98,07 N. The time of indentation was 10 seconds, for which the applied load is kept at a constant value. These factors give the subsequent Brinell hardness represented in the following form: *xxx HBW 1/10/10*. Brinell

hardness is calculated from the factors given above and of the mean indentation diameter ( $d$ ) as shown in equation (4):

$$HBW = 0,102 \frac{2F}{\pi D^2 \left(1 - \sqrt{1 - \frac{d^2}{D^2}}\right)} \quad (4)$$

As object lenses for the half-automatic analysis of indentation a magnification of 178x was used. According to standard, the minimum thickness of specimens must be 8 times of depth of indentation, which would be in this case a thickness of at least 0,51 mm. This limit could be met with all specimens, since the probe with the shortest cross section length was the rectangular die, with a height of 4 mm. Testing had to be done on a plain surface, so all specimens were mechanically polished before testing. Testing was conducted at ambient temperature. Furthermore, the applied force has to be selected in a way, that the indentation diameter is in the range  $0,24 \cdot D \leq d \leq 0,6 \cdot D$ . The indentation diameter is calculated as a mean value out of two perpendicular measured diameters from the impression form. The hardness is automatically determined by the testing machine software. With a measured hardness in the range of 50 – 105 HBW for the examined specimens, the indentation diameter meets the required criterion with the applied force.

Specimens of the rectangular die form were tested in short transverse direction (ST) 5 times and in longitudinal direction (L) 3 times, whereas specimens of the square die form were tested 3 times in ST- and 5 times in the L direction<sup>3</sup>. Overall hardness in section 5.5 is calculated as the mean value of all measurements in both directions for each specimen. For all specimens, the required distance of  $\geq 2,5 \cdot d$  from specimen edges and  $\geq 3 \cdot d$  from other indentations was kept according to standard.

---

<sup>3</sup> Short transverse direction is oriented perpendicular to the longitudinal transverse plane, longitudinal direction is oriented perpendicular to the short transverse plane.

## 5 Results and discussion

### 5.1 Pre-heating characteristic of billets

The oven temperature was varied in steps of 480°C, 550°C and 600°C for the first test series AH1 to AH5. The heating was conducted from ambient temperature until the core temperature of billet reached 450°C, 480°C and 480°C respectively. As can be seen in Figure 19 and Figure 20, generally there is just a small gradient between core and surface temperature. This can be explained by the high thermal conductivity of aluminium alloys [4] and also by the small billet volume (135 cm<sup>3</sup>). Merely the test series AH3 showed a significantly higher heating rate on the surface at the beginning. Still, it matched up with core temperature after 40 minutes. The first two test series at 480°C oven temperature (AH1 and AH3) show a divergence of approximately 10°C in maximum temperature. This difference is probably due to the fact, that between these two tests both thermocouples were newly positioned in the bore (core temperature) and on the surface of the billets. It can be concluded, that the exact position of thermocouple tip might have changed a little. Furthermore, less usage of ceramic paste from AH3 onwards may have improved contact of thermocouple contact point with the billet too. Throughout the subsequent test runs, the fixation of thermocouples stayed the same. Due to the heating characteristic of the billets during the first test series, oven temperatures in subsequent experiments (AH6 – AH10) could be further increased, without risking partial material melting on the surface.

In Figure 20 all heating curves that are shown, were measured with an oven setting of 600°C. The first two curves (AH6 and AH7) were probably faulty measurements, as explained in section 0. The remaining heating curves AH8 – AH10 are in good accordance with measurements from first test series as well as with calculated heating time due to model (see section 0). With this second set of tests, two different goals were achieved: first it was a verification of first test series measurements. Second, the influence of different positioning of probes in the oven was checked. Considering that AH9 was positioned more in the centre, and AH10 more in the front of the furnace, and that heating curves superpose each other, probe position does obviously have no impact on heating.

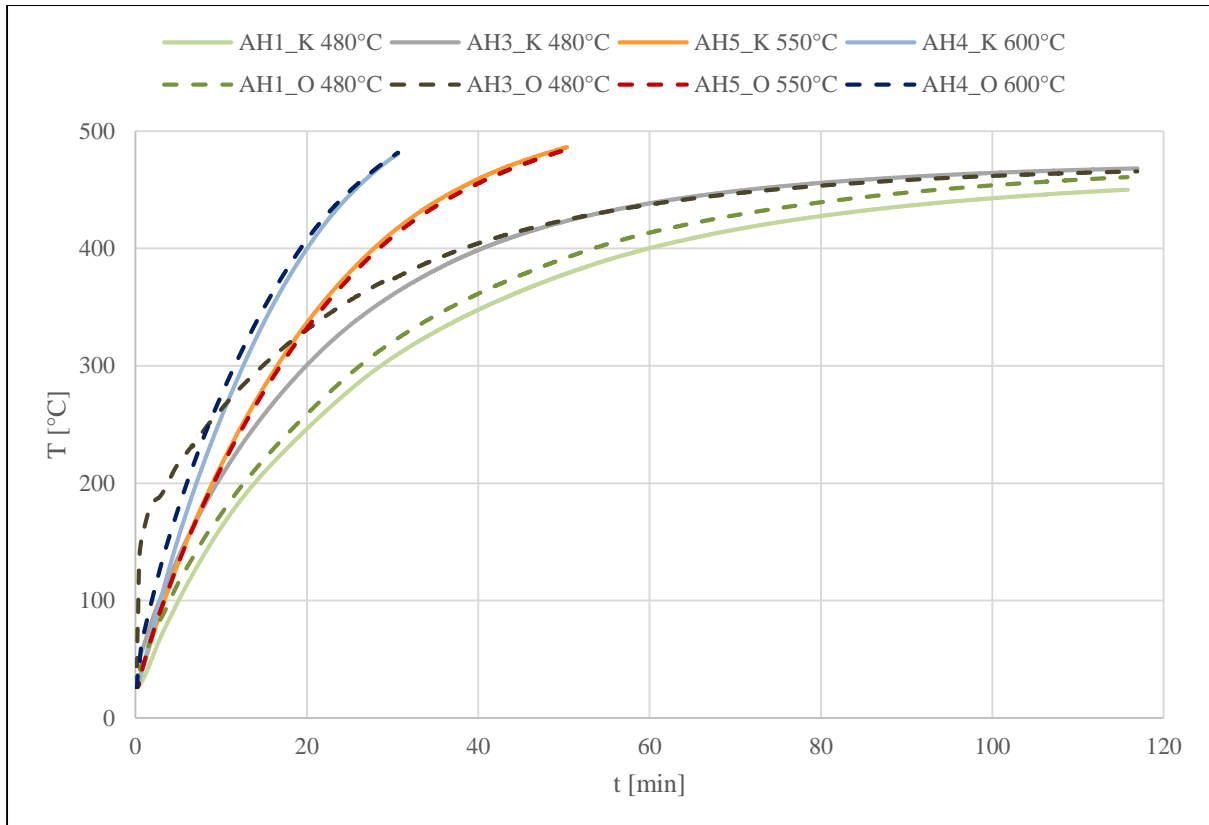


**Figure 19: Measured billet temperatures in comparison surface to core for varying furnace temperatures, test series AH1 – AH5.**

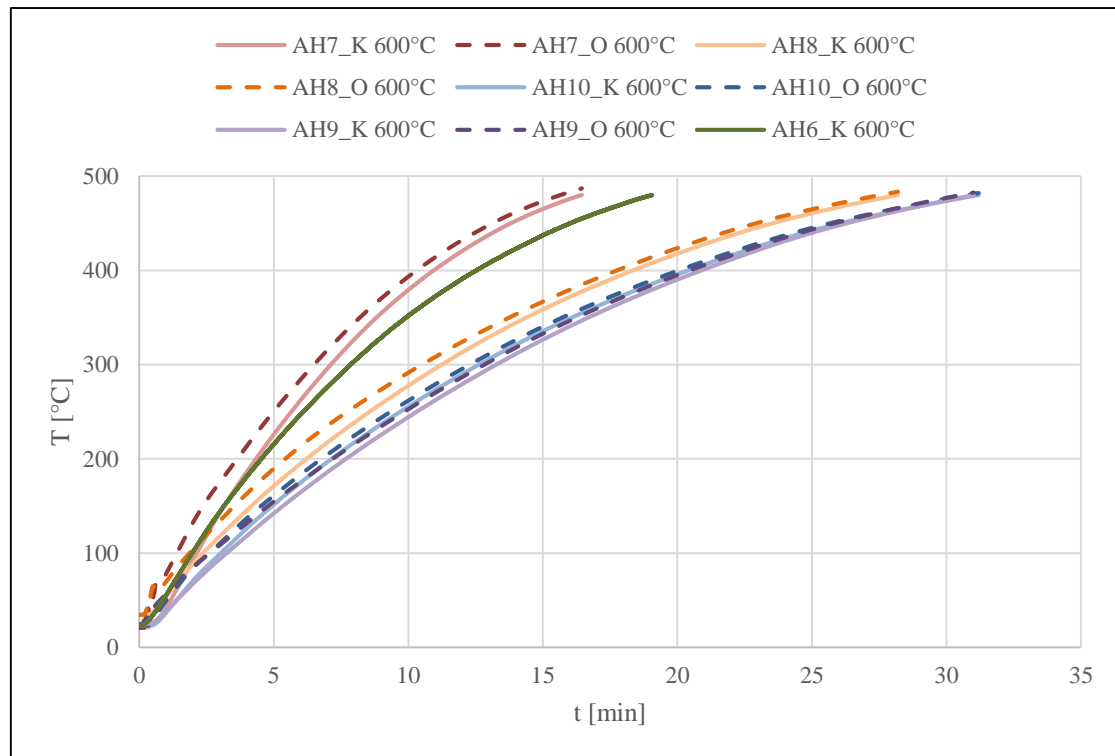


Figure 20: Temperatures of billet surface and core for test series AH6 – AH10 at 600°C oven temperature.

Error of furnace and thermocouples:

One objective for future application of this laboratory system was to determine the accuracy of heating equipment. Accuracy and acceptable errors for thermocouples of all types are stated in standard EN 60584-1:2013 [36]. For thermocouple type K, usable in the temperature range from -40°C to 1000°C, the tolerance lies within either equation (5) or (6), depending on which equation gives the higher tolerance value. For the system at hand, the tolerance at 480°C for the thermocouple can be +/-1,9°C, according to equation (6).

$$Tolerance = \pm 1,5^{\circ}C \quad (5)$$

$$Tolerance = \pm 0,0040 \cdot |T| \quad (6)$$

To determine any deviations of the furnace, one experiment with a 1 cm<sup>3</sup> small cube of aluminium was conducted in reference to a standard billet to minimise the effect of heating lag due to material volume. The cube was heated alongside a billet with dimension as billet 1 (see Figure 13(a)), only, this time the thermocouple was positioned at the axial centre of the billet cross section, 33 mm from the top surface. The thermocouple in the billet was fixated again with the ceramic paste, whereas fixation in cubic body was accomplished by screwing down the thermocouple wire with a small splint in the bore hole. The two bodies were first heated up to 480°C, subsequently to 500°C oven temperature. The final stages of the heating curves are shown in Figure 21(a) and (b).

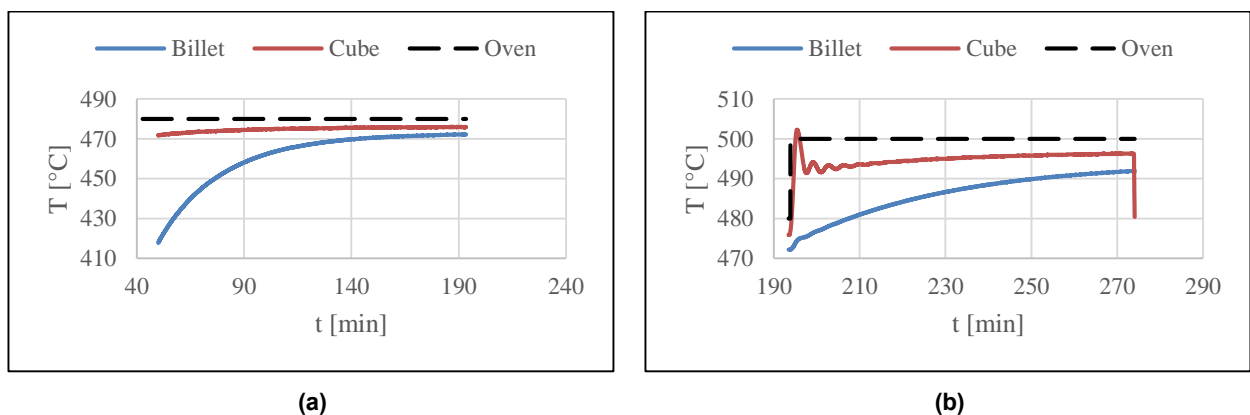


**Figure 21: Temperature deviations oven to core when heating the oven to: (a) 480°C and (b) 500°C.**

As can be seen in both figures, core-heating of the billet lags behind the cubic body, which can be explained by much less material volume of the cubic specimen. Both graphs also show a constant deviation of the maximum core temperature in comparison to the furnace temperature, although cube temperature was always higher than the billet temperature. That may be explained by worse contact of thermocouple, i.e. heat conductivity of ceramic paste compared to the fixation with a splint. Table 6 shows a constant deviation of -4°C for the core temperature of the cube. Considering the tolerances for thermocouples mentioned earlier in this section, this means that the heating error of the furnace lies within a range of -2 to -6°C, which implies a maximum error of 1,25% at a temperature level of 480°C. This experiment also showed the discrepancies for the chosen test setup as used in section 5.1 to measure heating rates for the billet. The system at hand showed a constant total error of 8°C core temperature for both temperature levels.

**Table 6: Temperature deviations for cube and billet during heating characterisation.**

	Heating [°C]	Heating [°C]	Deviation [°C]	Deviation [%]
Oven	480	500	-	-
Cube	476	496	-4	0,8
Billet	472	492	-8	1,6

For test series, two different types of thermocouples were used. For series AH1 – AH5 measuring was performed by thermocouples without special insulation, for series AH6 – AH10, type K thermocouples with a glass fibre insulation came to use. According to datasheets, usage of these glass fibre cable coatings is only approved up to +400°C. Temperature measurements beyond this limit also worked sufficiently, partly disintegration of the insulation caused a measured temperature increase for freshly installed thermocouples though. This resulted in faulty heating rates in series AH6 and AH7. Disintegration of the thermocouple coating can be seen by black spots in Figure 22(b) compared to the clean billet surface in Figure 22(a). It also shows the transformation to a white surface for the glass fibre coating.

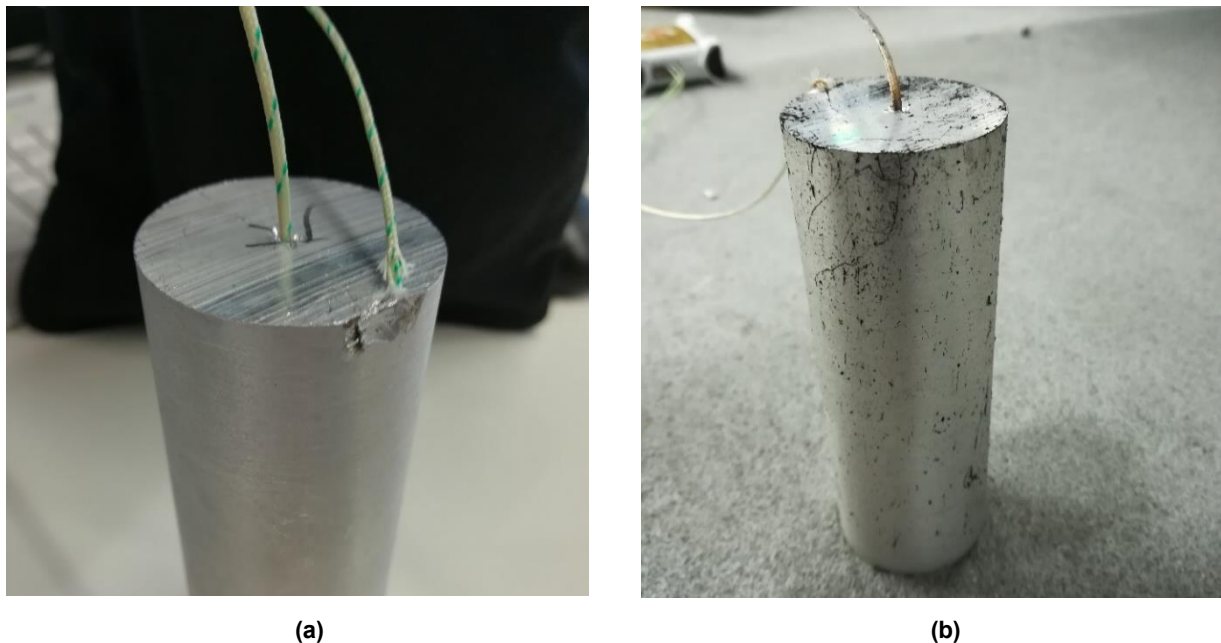


**Figure 22: Billet with thermocouples before (a) and (b) after first temperature test.**

Calculation of pre-heating time:

Implementing a simple model for calculating pre-heating time as a function of furnace temperature is useful in multiple ways: first it was an easy way to evaluate measured data. Second the proposed model gives the possibility to customize pre-heating time to user's needs. It should be mentioned, that the proposed calculation is sensitive to positioning of probes in the furnace as well as it is designed for the specific dimensions of used billets in this experiment. Pre-heating settings in subsequent extrusion series were solely chosen on basis of the time-/temperature model.

The model is based on the calculation of cooling time of a finite cylindrical body, as performed by Baehr and Stephan [37]. Equation (7) shows how heating time is calculated.

$$t = \ln(T^+) * \left[ -\frac{c * \rho * V}{\alpha * A} \right] \quad (7)$$

$C$  and  $\rho$  are material parameters, where  $c$  denotes the specific heat capacity and  $\rho$  the density of alloy AW6082,  $\alpha$  denotes the heat transfer coefficient.  $V$  is the volume of the billet and  $A$  is its surface. The only adaption made to the equation, is that for the calculation of body surface only cylindrical and top surface were considered, since there is no heat transfer through the bottom of the billet.  $T^+$  is calculated the following way:

$$T^+ = \frac{T_{Oven} - T_C}{T_{Oven} - T_0} \quad (8)$$

In equation (8),  $T_{Oven}$  denotes the selected oven temperature,  $T_C$  is requested core temperature of the billet after heating and  $T_0$  is the starting temperature (for experimental calculation it was selected as ambient temperature).

In case the oven temperature is needed with a given heating time, the equation is transformed like in (9):

$$T_{Oven} = \frac{e^{\left(-\frac{\alpha * A}{c * \rho * V * t}\right)} * T_0 - T_C}{e^{\left(-\frac{\alpha * A}{c * \rho * V * t}\right)} - 1} \quad (9)$$

Heat transfer coefficient  $\alpha$  is not a material parameter but defined by the nature of heat transfer and the geometrical constitution of material. For the system at hand the assumption is met that the heat transfer happens as natural convection between air and aluminium. Natural convection means, that there is just natural airflow, hence the oven does not provide a fan, just a simple deduction hole. Since there is little data for the value in literature ([38], [39], [40]), the heat transfer coefficient was determined experimentally for this specific system. Therefore, with heating data of already performed experiments, the parameter  $\alpha$  could be calculated out of altered equation (10).

$$\alpha = -\frac{c * \rho * V}{A * t} * \ln\left(\frac{T_C - T_{Oven}}{T_0 - T_{Oven}}\right) \quad (10)$$

The parameters used for heat transfer coefficient calculation are shown in Table 7. The median value was taken to define a final value  $\alpha$  of 18,1 for the system. With this temperature model, heating times could be sufficiently determined in the used temperature range from 480 – 600°C. For subsequent experiments usually oven temperature was set to 600°C for 32 minutes resulting in 480°C core temperature.

**Table 7: Parameters used for calculation of the empirical heat transfer coefficient aluminium - air.**

	t	T <sub>C</sub>	T <sub>Oven</sub>	T <sub>0</sub>	c	ρ	V	A	α
	[s]	[°C]	[°C]	[°C]	[J/kgK]	[kg/m <sup>3</sup> ]	[m <sup>3</sup> ]	[m <sup>2</sup> ]	[W/m <sup>2</sup> ]
AHV 2	4571	450	480	25	896	2700	0,000135	0,015022	12,9
AHV 3	4282		480	25					13,8
AHV 4	1830		600	25					18,6
AHV 5	2909		550	25					15,0
AHV 8	1692	480	600	35	896	2700	0,000135	0,015022	19,9
AHV 9	1860		600	25					18,3
AHV10	1872		600	25					18,1

## 5.2 Calculation of extrusion exit temperature

Temperature conditions during extruding are a key factor to uniform product quality and higher productivity. Due to high temperatures, flow stress is reduced and deformation of material becomes therefore easier and less energy consuming. Maximum temperature is restricted though, since extruding is a hot working process, which means beyond the eutectic temperature of material incipient melting may begin. Heat is generated mainly due to friction and deformation effects: billet-container interface friction, dead-metal zone-flowing metal interface friction, die bearing-material interface friction and work of deformation in front of the die in the deformation zone. Summarizing in a formula, these individual effects can be calculated according to Sheppard [14]:

$$\Delta T_1 = \frac{\bar{\sigma} * \ln(ER)}{\sqrt{3} * (\rho_{Al} * C_{p(Al)})} \quad (11)$$

Equation (11) shows heat that is generated during deformation processes ( $\Delta T_1$ ).  $\bar{\sigma}$  denotes the flow stress for AW6082 at 480°C. As for density and specific heat capacity, values are the same as in Table 7. In equation (12) temperature increases ( $\Delta T_2$ ) at billet surface as a consequence of friction to container wall is given. The equation additionally takes the ram speed ( $V_R$ ), billet length ( $L_B$ ) and thermal diffusivity ( $\alpha_{Al}$ ) into account. Thermal diffusivity is calculated as the quotient of thermal conductivity ( $\lambda$ ) and density multiplied by specific heat capacity.

$$\Delta T_2 = \frac{\bar{\sigma}}{4 * \sqrt{3} * (\rho_{Al} * C_{p(Al)})} * \sqrt{\frac{V_R * L_B}{\alpha_{Al}}} \quad (12)$$

Finally, the temperature increase ( $\Delta T_3$ ) due to friction between die bearing and material can be calculated the following way (13):

$$\Delta T_3 = \frac{\bar{\sigma}}{4 * \sqrt{3} * (\rho_{Al} * C_{p(Al)})} * \sqrt{\frac{V_E * L_D}{\alpha_{Al}}} \quad (13)$$

This equation contains now the exit speed of the extruded product  $V_E$  and  $L_D$  for die bearing length. Results for this heat generating equations in accordance with the used die geometries are shown in Table 8.

**Table 8: Different types of heat generation calculated for diverse die geometries. This table also contains the geometrical data and flow stress for every die form.**

	<b>RW</b>	<b>W10</b>	<b>W5</b>	<b>QW</b>	<b>[...]</b>
ER	17,3	16,0	35,3	13,9	-
$A_E$	80,0	86,6	19,6	100,0	mm <sup>2</sup>
$V_E$	812	750	1654	649	mm/s
$L_D$	8,5	13,5	8	5	mm
$\sigma$	75,8	75,5	78,1	74,9	MPa
$\Delta T_1$	<b>51,6</b>	<b>50,0</b>	<b>66,4</b>	<b>47,0</b>	°C
$\Delta T_2$	<b>36,0</b>	<b>35,9</b>	<b>37,1</b>	<b>35,6</b>	°C
$\Delta T_3$	<b>41,8</b>	<b>50,5</b>	<b>59,7</b>	<b>28,4</b>	°C

Although the absolute exit temperature cannot be determined by these equations, since all the heat effects superpose one another, Table 8 still gives a good overview, which heat generating mechanisms have a greater impact on overall temperature rise. As can be seen for all die geometries, the heat is mainly generated through deformation work of material. The two-hole diameter rods (W5), which have the highest extrusion ratio, also indicate the highest overall temperature rise. The input of deformation effect is 24% (QW) – 44% (W5) higher than friction from container wall. Generally, the influence of friction between container wall and billet seems to be the least heat generating factor. Only for the QW die geometry, the part of heat from die friction is significantly lower, which is because of the relatively slow extruding speed in combination with short die bearing, compared to the other geometries. According to Saha [26] some diagrams show a temperature rise of up to 100°C during the extruding process, especially for elevated ram speeds. Tough, more common is a temperature rise of around 40°C [6].

All above mentioned heat generating effects show a strong dependency to the specific geometric parameters. Since there is a strong dependency on ER, the temperatures of all dies show mainly different gradients for each calculation. Only  $\Delta T_2$  shows merely the same temperature rise for all dies, since calculation is essentially a function of container parameters. One parameter that influences all three heat effects is flow stress  $\bar{\sigma}$ . As already mentioned in

this section, this parameter is a function of temperature, but also of geometric aspects, such as strain ( $\epsilon$ ) and strain rate ( $\dot{\epsilon}$ ). Flow stress for a temperature of 480°C was also determined via calculation, according to Sheppard [41]:

$$\bar{\sigma} = \frac{1}{\alpha} * \ln \left\{ \left( \frac{Z}{A} \right)^{\frac{1}{n}} + \left[ 1 + \left( \frac{Z}{A} \right)^{\frac{2}{n}} \right]^{\frac{1}{2}} \right\} \quad (14)$$

Parameters used in equation (14) are shown in Table 9.  $A$ ,  $\alpha$  and  $n$  denote constants for this equation for the AW6082 alloy.  $Z$  denotes the Zener-Hollomon-parameter, as described in equation (15):

$$Z = \dot{\epsilon} * e^{\left( \frac{\Delta H}{GT} \right)} \quad (15)$$

The Zener-Hollomon-parameter was developed as a temperature compensated strain rate that correlates strain, strain rate and the influence of temperature. In this equation,  $\Delta H$  denotes the activation energy,  $G$  is the universal gas constant and  $T$  the absolute temperature. Values for constants  $A$ ,  $\alpha$  and  $n$  of alloy AW6082 are also given in literature source [41]. Magnitude of  $Z$  with strains from 2,6 – 3,6 (Table 11) is in good accordance with  $Z$ -values for other 6xxx alloys [42].

**Table 9: Flow stress for all die geometries at 480°C, according to individual strain rates.**

	<b>RW</b>	<b>W10</b>	<b>W5</b>	<b>QW</b>	<b>[...]</b>
$\dot{\epsilon}$	18,9	19,1	25,6	16,9	s <sup>-1</sup>
<b>Z</b>	7,73·10 <sup>11</sup>	7,8·10 <sup>11</sup>	1,05·10 <sup>12</sup>	6,9·10 <sup>11</sup>	
<b>Z/A</b>	3240	3269	4391	2891	
$\bar{\sigma}$	<b>75,8</b>	<b>75,9</b>	<b>78,1</b>	<b>74,9</b>	<b>MPa</b>

### 5.3 Evaluation of extrusion ratio and strain rate

The equations in this chapter are all based on the book “Aluminium Extrusion Technology” [26]. The extrusion ratio (ER) is an important variable concerning the required force for the extrusion

process and material quality of extruded product. ER is calculated as the quotient of container cross-sectional area ( $A_C$ ) and extruded cross-sectional area ( $A_E$ ), with  $n$  as number for multi-hole dies, as shown in equation (16):

$$ER = \frac{A_C}{n * A_E} \quad (16)$$

Extrusion ratios for the used die geometries are shown in Table 10. Only the QW-die is a multi-hole die, consisting of two round holes. According to Saha [26], ER for soft grade aluminium alloys (such as AW6082) should be in a range from 10 – 100. The higher the ER value gets, the higher is the global deformation of metal. Though, depending on specific die geometry, a high local deformation degree could also occur while having a relatively low extrusion rate. That is for example the case for the QW die: light microscopy analysis showed a recrystallized coarse grain structure over the entire circumference, due to high temperatures during extrusion. As explained in the previous section 5.2, this rise in temperature partly occurs due to a high degree of deformation. On the contrary, photomicrographs of the RW-die, which has a higher ER than QW-die, showed no signs of any coarse grain in the mid area of the LT -plane, meaning there is less temperature development during the process with the same processing parameters.

**Table 10: Extrusion ratios for different die geometries.**

	<b>RW</b>	<b>W10</b>	<b>W5</b>	<b>QW</b>	<b>[...]</b>
<b>A<sub>C</sub></b>	1385,4	1385,4	1385,4	1385,4	mm <sup>2</sup>
<b>A<sub>E</sub></b>	80,0	86,6	19,6	100,0	mm <sup>2</sup>
<b>ER</b>	17,3	16,0	35,3	13,9	-

Deformation is usually described as the natural strain ( $\bar{\epsilon}$ ), as given in equation (17):

$$\bar{\epsilon} = \ln(ER) \quad (17)$$

As can be seen, natural strain is a function of ER. In its definition, the natural or logarithmic strain is the logarithm of the quotient of final length to initial length. As the volume of material has to be constant for the entire process, the ratio of lengths could be replaced by ratio of cross-sectional areas, which is per definition ER.

Calculation of the strain rate is more complex, since it is also a function of dead metal zone semiangle ( $\alpha$ ), which could not be measured directly. An equation to determine  $\alpha$  is shown in (18).  $D_C$  is the container bore,  $D_E$  the equivalent diameter of the extruded rod and  $L$  the length of the deformation zone, as shown in Figure 23.

$$\alpha = \arctan\left(\frac{D_C - D_E}{2 * L}\right) \quad (18)$$

In direct extrusion, the butt of the extrudate is usually not used for the final product, since material properties differ noticeably from the rest of the section. This may happen because of oxides or other contaminations polluting the extrusion. Saha [26] claims that industrial standard for butt thickness in direct extrusion is kept to 10 – 15% of billet length. The dead metal zone semiangle, that defines the deformation zone, is influenced by many factors, such as ER, type of die, billet temperature, billet container friction condition or flow stress. Usually butt thickness is chosen as length of deformation zone plus a safe margin. But for a basic assessment of strain rate, the safe margin is neglected and the length of deformation zone is assumed to be 15% of the billet length, which makes a determination of  $\alpha$  possible. The mean effective strain rate can be determined according to equation (19):

$$\dot{\bar{\epsilon}} = \frac{6VD_C^2 \tan \alpha}{D_C^3 - D_E^3} * 2 \ln \frac{D_C}{D_E} \quad (19)$$

All values for the different die geometries used are shown in Table 11.

**Table 11: Natural strain, strain rates and length of extrudates for different die geometries.**

	<b>RW</b>	<b>W10</b>	<b>W5</b>	<b>QW</b>	<b>[...]</b>
<b>ER</b>	17,3	16,0	35,3	13,9	-
<b>D<sub>E</sub></b>	10,1	10,5	7,1	11,3	mm
<b><math>\alpha</math></b>	44,3	43,9	46,9	43,2	Grad
<b><math>\bar{\epsilon}</math></b>	2,85	2,77	3,56	2,63	-
<b><math>\dot{\bar{\epsilon}}</math></b>	18,9	18,2	25,6	16,9	s <sup>-1</sup>
<b>L<sub>E</sub></b>	1888	1744	3846	1510	mm

Table 11 also contains the theoretical length of extrudate ( $L_E$ ) which is based on the concept of volume consistency of metal.  $L_E$  is simply calculated as the product of billet length and ER. For the W5-die, each of the two-hole extrudates measures 3,85 metres.

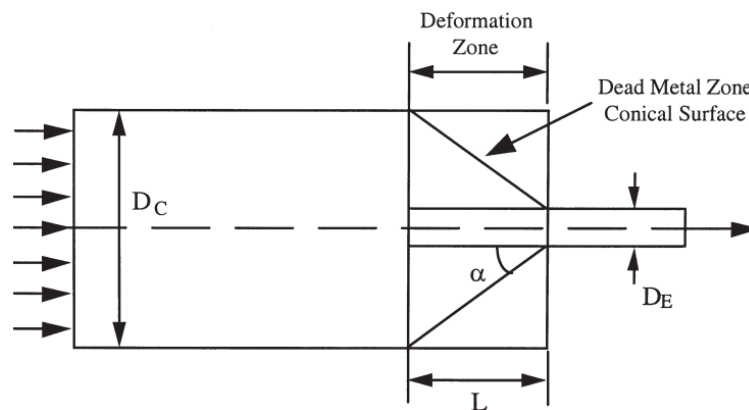
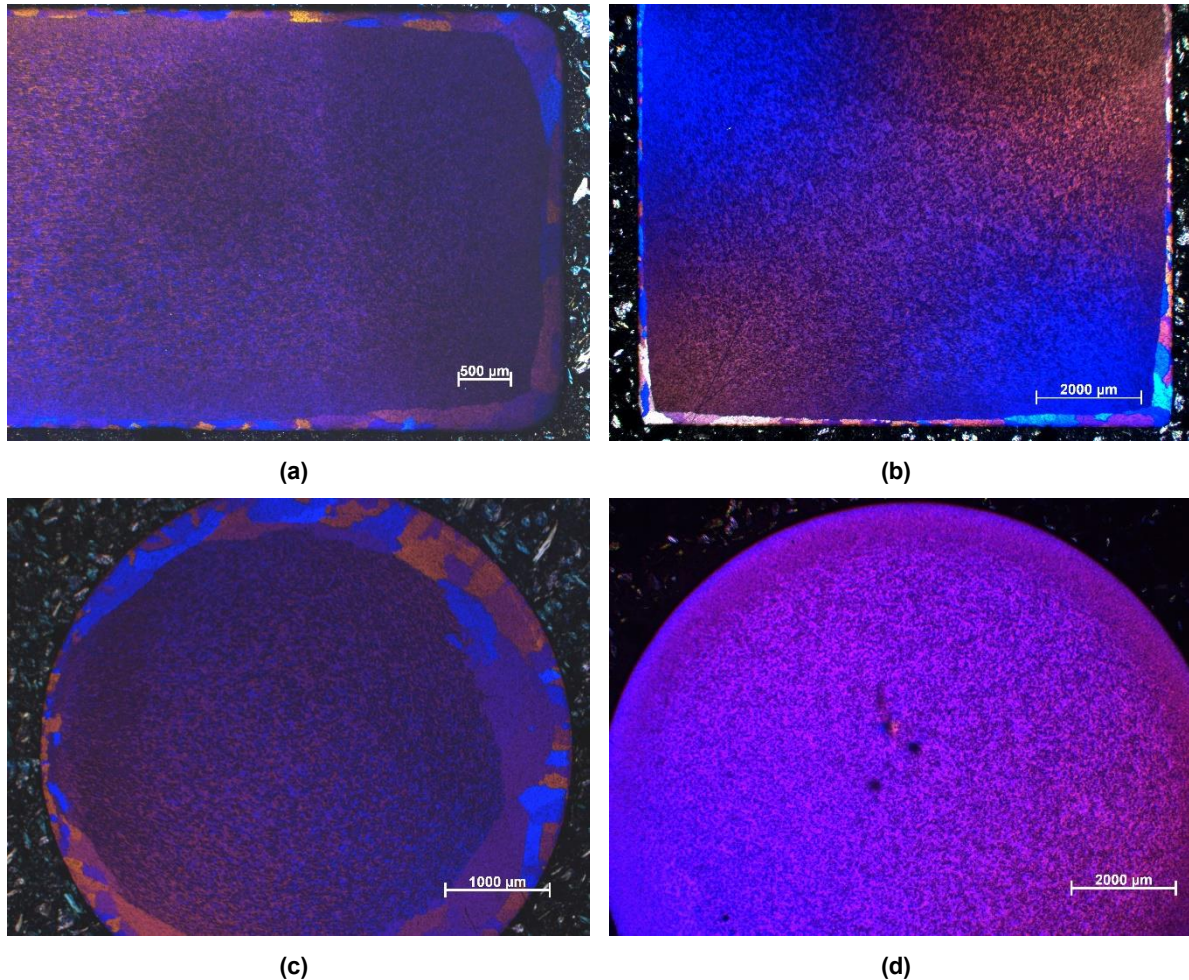


Figure 23: Billet geometry inside the container [26].

#### 5.4 Influence of die geometry on the extrudate microstructure

Light optical microscope analysis of grain structure for the different die geometries can be seen in Figure 24(a) – (d). Except Figure 24(d), which shows the cross-section of the W10-die, all cross-sections show some peripheral coarse grain and fine grain in the centre. For the W-10 sample the reverse is the case: grains at the periphery seems to be finer than in the centre. According to Parson [18] the structure with fibrous core and peripheral coarse grain (Figure 24(a) – (c)) for this alloy is reached with high extrusion speed and medium grade temperatures. Both aspects can be confirmed for these experiments. Although ER of W5-die is much higher than the ones of RW- and QW-die, the latter two also recrystallize in the outer band. This is also because of a locally high degree of deformation, as for example at the corners of the die, where the layer of coarse grain is thicker than on the longitudinal sides. The flowing material has generally to undergo a larger deformation on the surface than in the billet centre, resulting in a higher rate of dislocations. Hence the stored energy to initiate nucleation of new grains is mainly concentrated at corners or surfaces. As for the W10-die it is assumed that the overall deformation is not as high as with the other geometries, although ER is similar. Because of the relatively large die diameter and the rod form there are no such high local deformation values as for the cube-shaped extrudates. It seems, that peripheral coarse grain is in this case coupled

with either a high ER or with a more complex geometry, i.e. rectangular form with corners in comparison to round bars.



**Figure 24: Cross-section polish of all dies, with billets being pre-heated to 480°C: (a) RW-die at 25x magnification, (b) QW-die at 12,5x magnification, (c) W5-die at 25x magnification and (d) W10-die at 12,5x magnification.**

### Stretching of grains:

As already shown in Table 11, the extrusion process generates high natural strains in the material of up to 3,56. This deformation also takes place microscopically in stretching of grains. While the peripheral grain recrystallizes and therefore does not undergo an extreme stretching mode, the inner, finer grains experience a considerable elongation. Optical light microscopy pictures demonstrated this strain of grains but were not suitable for a quantitative evaluation of the degree of deformation. Hence, the impact of die geometry on stretching of grains is compared qualitatively. Figure 25 shows a longitudinal cross-section image of a W10-die (a), a QW-die (b) and the W5-die form (c). In Figure 25(a) and (b) grains are coarser in the middle of

the extrudates and become finer towards the outer rim, with the only real difference being the peripheral coarse grain at the QW-die. As for longitudinal stretching, grains seem to be a little bit longer for the QW-die than for the W10-die throughout the whole cross-section. Grains of the W5-die (c) on the other hand seem to be of a similar length (except peripheral coarse grain), though they appear even finer than elongated grains of W10- and QW-form. The reason for this appearance is due to extrusion ratio, which is more than twice the value for the W5-die, which naturally also means more than double length of extrudates from W5-die compared to the other die forms.

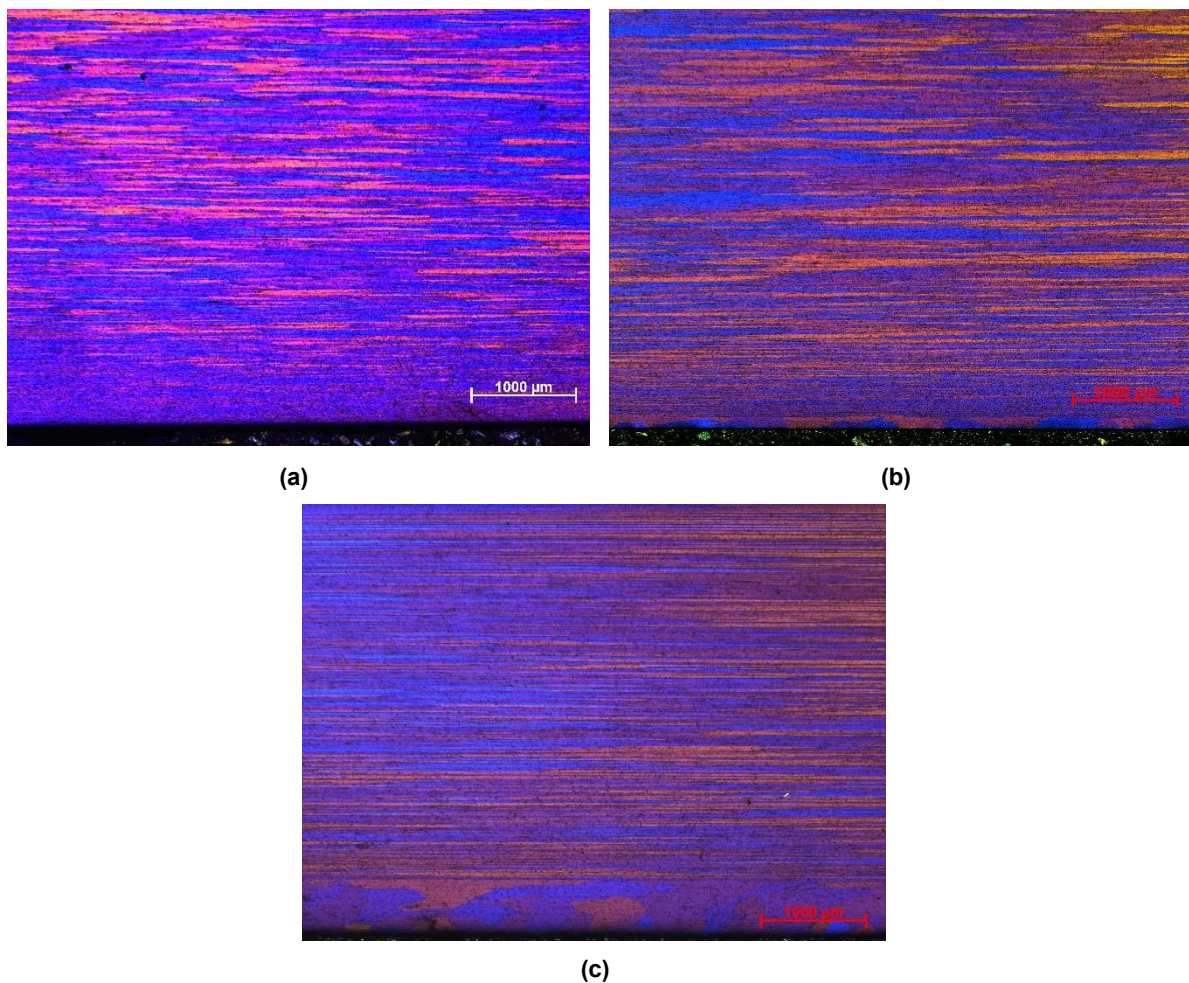


Figure 25: Comparison of grain elongation for extrudates of (a) W10-die, (b) QW-die and (c) W5-die at 25x magnification.

## 5.5 Influences of different thermal routes

In this section, results of the different heat treatment steps and the impact of die geometry on mechanical properties will be discussed. The exact procedure of thermal routes has already been described in section 4.3.

In Figure 26 hardness is shown for products extruded with the QW die and a pre-heating time of 480°C with all thermal routes that were tried out. As can be seen, extruding with slow cooling rates and natural ageing afterwards (T5 for 3h and 6h) show no significant effect on hardness compared to the T1<sup>4</sup> state. The same applies to T6 tempered extrudates that were only solution annealed for 5 minutes. Apparently, this period at annealing temperature was not long enough to bring sufficient Mg-Si particles in solution, resulting in fewer precipitates, i.e. no possibility for precipitation hardening. On the contrary, with the specimens that were annealed for 30 minutes, even the non-aged sample showed a considerably increase in hardness. Following an artificial ageing step of 5 hours, hardness could be maximized to a value of 105 HBW 1/10, which is twice as high as in the prior T1, T5 and T6 states. This value is also in good accordance to standard DIN EN 755-2 [2], which demands a hardness of 95 HBW for bars with a width across flats  $\leq 20$  mm in the T6 temper.

---

<sup>4</sup> T1...Cooled down from elevated temperature after forming followed by natural ageing to a widely stable material condition.

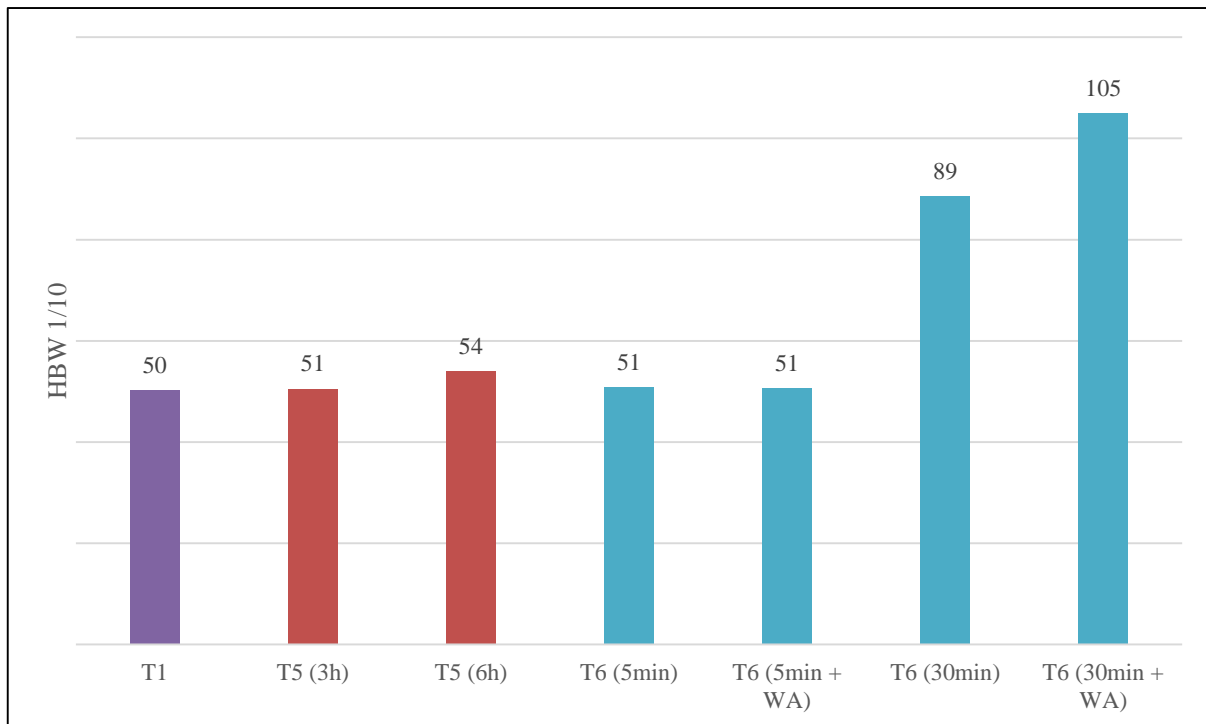


**Figure 26: Hardness of products in the QW-form for thermal routes T1, T5 and T6 with different solution and ageing times.**

In Figure 27 Brinell hardness is illustrated for the RW-die form in the three pre-heating conditions. Clearly, there is no difference in hardness for the 420 and 480°C specimens. The 540°C step shows a slight increase for all tempers though. Given the fact that the particular tempering had little influence on hardness, the correlation of increasing hardness with increasing the pre-heating temperature is obvious. This suggests that with the highest pre-heating temperature there should also be a rise in dissolved Mg- and Si-particles that increase the number of precipitates at least for a small degree. This can be concluded, because starting from a billet temperature of 540°C plus adding the heat generation during extruding the material should easily exceed the solvus temperature.

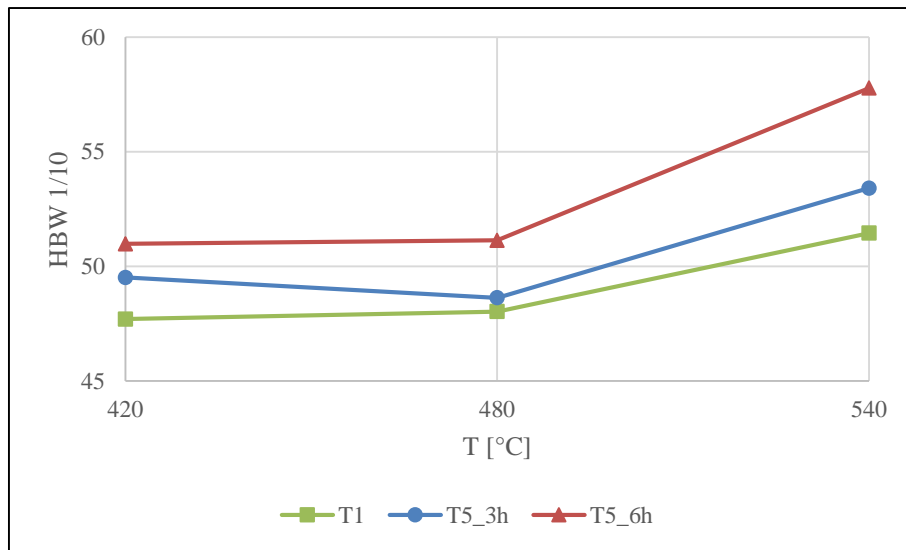


Figure 27: Influence of pre-heating temperature on product hardness for RW-die.

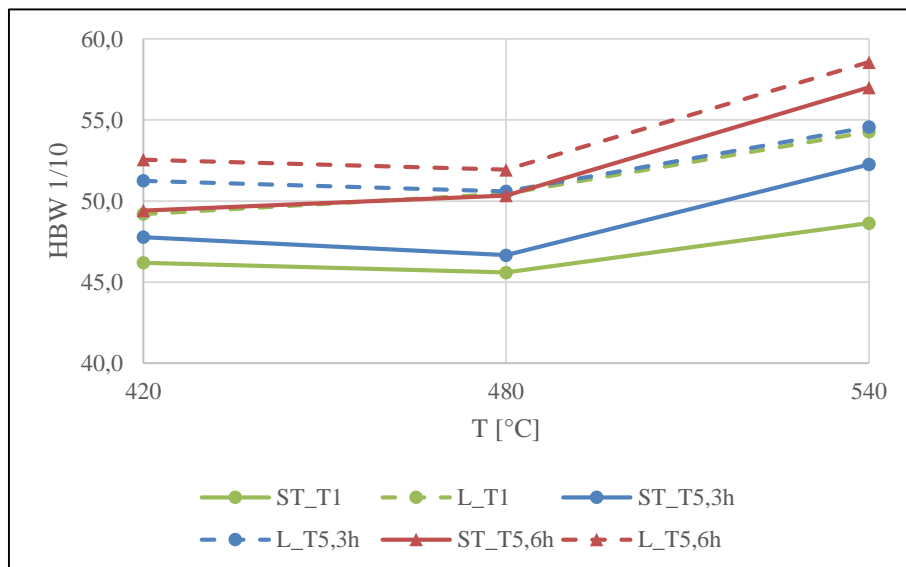


Figure 28: Hardness for different pre-heating temperatures and thermal routes, measured from longitudinal- and from short transverse direction of RW-extruded product.

In Figure 28 Brinell hardness is shown again for the three pre-heating regimes, but this time with curves for measurements either on the longitudinal top surface (short transverse (ST) direction - solid line) or on the cross intersection (longitudinal (L) direction - broken line) of the RW-die. The hardness for each tempering is slightly higher in the longitudinal- than in the short transverse direction. This might be explained by the recrystallized grain structure and texture of the material. When testing in short transverse direction, all spots on the extrudate surface contained of the

more or less thin coarse grain layer, whereas when testing in longitudinal-direction, measuring points were right in the centre, with the fibrous elongated grains predominating. Usually finer grain sizes have higher strength, because of the higher density of grain boundaries, which likely built a barrier for dislocation movement. Measurements at the rim of cross-section were not possible, because the coarse grain layer was too thin and having a measurement this close to the edge might have falsified the results.

Also, according to [4] during hot- or cold-working procedures such as extrusion, random grain orientation from casting is changed in a preferred orientation. This texture shows anisotropic characteristics, resulting in an increase in strength in pressing direction.

In Figure 29(b) the cross section of a QW extrudate in the T6 temper after 30 minutes annealing time is shown. The round spots on the left side are artefacts from Barker etching. In this figure the peripheral coarse grain that came along with all pressings for this die form can be guessed. This outer rim of coarse grain reflects dynamic recrystallization during the process. The outer coarse grain layer seems to be a little bit thicker than without the annealing step (compare to Figure 29(a)). Grains may be coarser in the outer rim, because of two reasons: first, the cooling rates of pressed material are slow, leaving the material at elevated temperature for a longer time period and enabling the recrystallized grains to grow further. Second, this process also likely continued at the subsequent 30 minutes annealing. In both scenarios motion of grain boundaries is likely hampered by numerous dispersoids, as a result of the relatively high content of Mn and Cr in this alloy (see Table 2) [18].

Due to the subsequent solution annealing, there is also an inner area of extreme coarse grain recrystallizing. This area covers approximately half of the cross section. The deformation degree is high enough and time at the elevated temperature long enough for grains to grow to a significant extent. This is also in agreement with [18], which states that the already recrystallized outer rim is not really sensitive for any further heat treatments, but non-recrystallized zones are unstable and often affected by static recrystallization.

There is just the inner core left in a non-recrystallized state. Deformation decreases with closeness to the billet core since material does not need to flow as much in this area of the cross section, and strain and strain rates are of lower grade than near the billet surface. Thus, the grade of stored work is lower. Moreover, these loci experienced less heat development due to lack of friction. Overall, the locally decreased strain is not sufficient for this zone to recrystallize

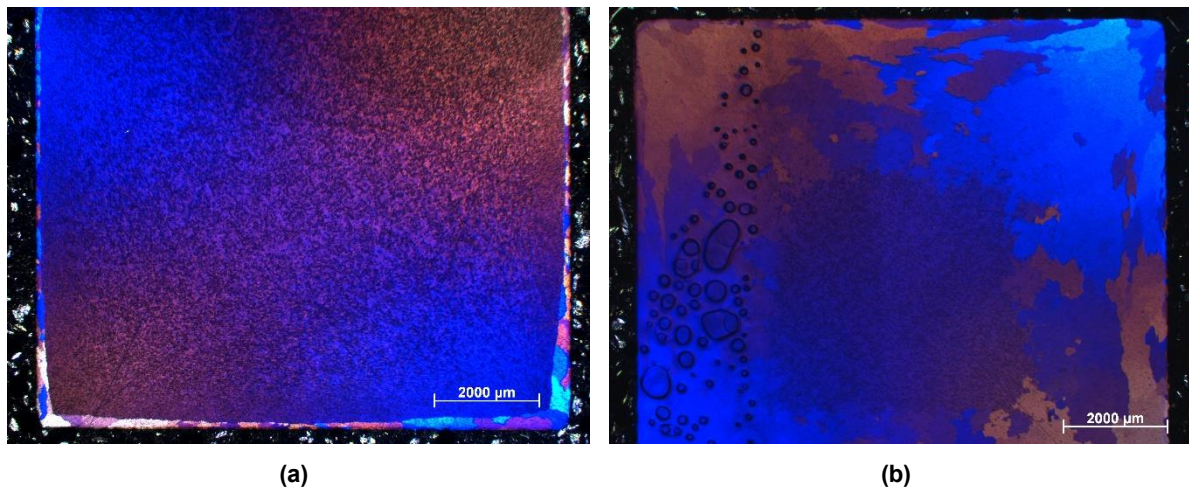


Figure 29: QW-product in T6 temper, with also recrystallized coarse grain in the inner section and just a small un-recrystallized section of fine grain in the center (a) and (b).

## 5.6 Dispersoids

Particularly dispersoid particles of AlFe(Mn)Si-type, together with other Mn- and Cr-rich particles show great importance to the extrusion process. They are believed to have a positive delaying effect on dynamic recrystallization, but on the other hand increase resistance to deformation, thus increase energy consumption of extrusion.

In Figure 30(a) the cast and homogenized material is shown. Primary AlFeSi-phases can be seen in elongated black form (red mark), essentially attached to precipitate free zones (PFZ – green mark). Figure 30(b) shows the short longitudinal plane of an extruded QW-bar and (c) again the ST-plane of the extrudate. Pictures were all taken in the fibrous mid-section of the bar, with a magnification of 500 times. Figure (b) indicates, that PFZs are stretched due to extrusion, if there are no adjacent dispersoid particles. Dispersoids themselves were barely affected by any elongation, though they seem to get oriented in extrusion direction, when comparing figure (c) to (a). In (b) dispersoids have a similar length as in (a), while in (c) the prior-to-extrusion needle-like form (from Figure 30(a)) is mainly gone, which indicates, that they have changed orientation in the direction of extrusion.

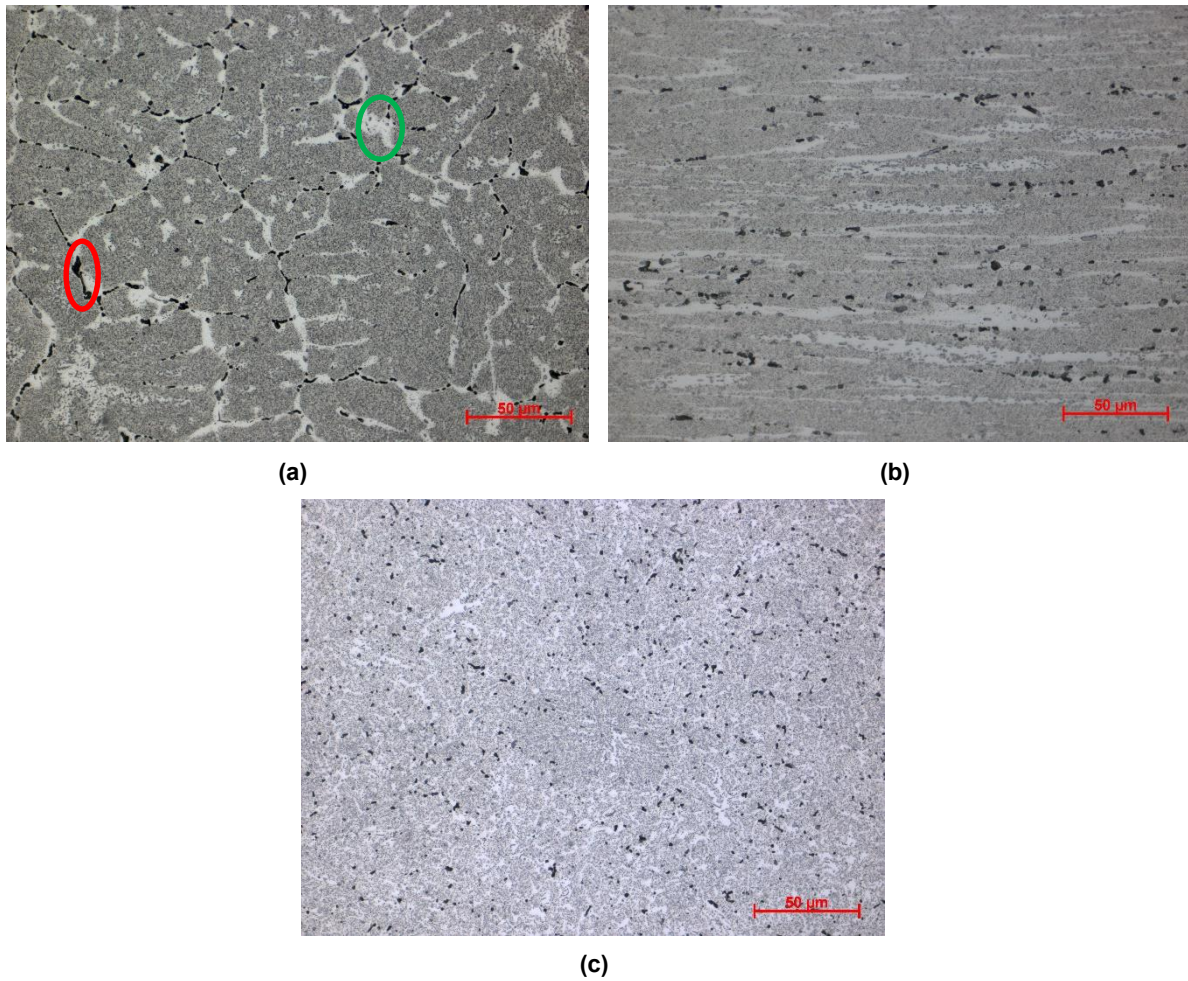


Figure 30: Light optical microscope pictures show dispersoids in (a) cast and homogenized form, (b) longitudinal section of extrudate and (c) cross section of extrudate. All figures were taken at 500x magnification.

## 6 Summary and Conclusions

The main goal of this thesis was to test and gain knowledge of the laboratory extrusion press, and in this context, be able to repeatedly produce extrudates of different geometries. Though there are many parameters that are relevant for the extrusion process, just five factors could be reasonably adjusted: pre-heating temperature of billets, ram speed, die geometry, die heating and tempering after extrusion. All experiments were conducted with billets of an AW6082 alloy.

First, pre-heating in the laboratory furnace was investigated. Billets were equipped with thermocouples, measuring temperature in core and on the surface. Due to good thermal conductivity of the material, heating time could be reduced to 32 minutes to reach a billet temperature of 480°C, when superheating the oven to 600°C and still avoiding incipient melting of the alloy. Heating-tests were checked by calculation, establishing a model for estimating heating time as a function of furnace temperature. Different pre-heating temperatures of 420, 480 and 540°C showed a minor impact on hardness for the given process setup. Increasing temperature also increased hardness but carries the risk of material getting too hot during pressing and resulting in a faulty end product.

Four different die geometries (RW, QW, W5, W10) were tested on functionality. With adequate pre-heating temperature (480°C), all dies could be used without difficulty. Except for the W10-die, all other forms showed peripheral coarse grain in a recrystallized zone in the extrudate cross section. This is caused by high ram speed of the press of 47 mm/s, which increases strain rates and heat generation and thus influences the degree of recrystallization.

Block-on-block pressing of billets was possible, however pre-heating of the die is necessary to perform this operation successfully.

Finally, possibilities of tempering for the AW6082 alloy in the course of the process were tested. Light optical microscopic analysis of microstructures indicated that not enough Mg-Si particles went into solution during extrusion which hampered sufficient supersaturation of the Al-matrix for precipitation strengthening during subsequent ageing. By interposing an annealing step at 560°C for 30 minutes prior to artificial ageing treatment, Brinell hardness was doubled from around 50 to 105.

## 7 Outlook

During test runs, especially furnace characteristics for pre-heating and handling of the press could be well understood. Nevertheless, a couple of factors appeared, that have a major impact on end product quality and are worth considering to be taken care of:

Successful thermal treatments within this study indicate that tempering is possible in the present test rig configuration. In current adaption, a runout table with integrated quenching system is being constructed and will be installed, which will give the opportunity to either cool with an air fan or water quench in a tank and thus better control cooling rates. This will further adapt the laboratory press to industrial standards and allow comparability with industrial scale presses. Moreover, a runout table will automatically straighten the extrudates, which is useful when using specimens for further investigations, for example, as dilatometer samples.

Furthermore, billets for this thesis were provided by the project partner *Neuman Aluminium Strangpresswerk GmbH* in homogenized condition. At the stage where the thesis started, basic parametrisation for usability of the press was the primary goal. Therefore, homogenization practise and subsequent cooling rates did not need to be further specified. With respect to the importance of this thermal treatment (as discussed in section 0) to the extrusion step, the specific homogenization practice should be considered in the future, to improve the overall extrusion process on an advanced level.

Repairing the ram speed rotary switch is mandatory in order to gain slower extrusion speeds. Reducing the ram speed will be the key factor to a uniform and fine microstructure and avoidance of coarse grain zones. In addition, it will give vast possibilities in process management and will offer the prospect of upscaling the extrusion machine to industrial applications.

Another option to reduce coarse grain that has already been realised in the course of this thesis was the design of an adapted rectangular die. The new die design uses a shortened die bearing length, with the effect of less heat generation because of lower friction surface.

A problem that occurred during work for this thesis was characterisation of microstructure. Light optical microscopy was sufficient for representing the formation of coarse grain and to determine its peripheral layer thickness. Although multiple etching methods were tried, it was not possible to determine a mean grain size of fine grains in the mid-section according to standards because of limited potential of resolution. Also, stretching of grains in longitudinal direction could not be quantified. For this purpose and to quantitatively compare extrusion parameter setups in the

future, it will be crucial to subject specimens to an EBSD analysis, and to determine microstructural changes after pre-heating, extrusion, and artificial ageing by electron microscopic analyses.

To better understand the phenomenon of the peripheral coarse grain zone, it would be interesting to calculate / simulate the local deformation at the periphery of the billet. Strain and strain rates in this thesis are mean values for overall deformation, but as shown in section 5.4 the die geometry has locally a great influence on recrystallization. Moreover, retardation of the billet surface in the container leads to different material flow regimes (billet surface and core) during extrusion. To quantify these local differences by means of simulation could help to understand the effect of limited recrystallization.

Finally, it would be of interest to analyse the transition at the interphase of fine fibrous to coarse grain. Especially regarding the role of dispersoid particles at this transition line, there exists little knowledge. In this context it will be required to target-prepare the transition line for subsequent analyses with electron microscopic characterisation.

## 8 References

- [1] I. Polmear *et al.*, *Light Alloys: Metallurgy of the Light Metals*, 5th ed., vol. 21, no. July. Matthew Deans, 2017.
- [2] “DIN EN 755-2:2016 Stranggepresste Stangen, Rohre und Profile - Mechanische Eigenschaften.” 2016.
- [3] “DIN EN 573-1:2004 Aluminium und Aluminiumlegierungen - Chemische Zusammensetzung und Form von Halbzeug - Teil1: Numerisches Bezeichnungssystem.” 2004.
- [4] F. Ostermann, *Anwendungstechnologie Aluminium*, 3. Auflage. Berlin, Heidelberg: Springer Vieweg, 2014.
- [5] “DIN EN 573-3:2013 Aluminium und Aluminiumlegierungen - Chemische Zusammensetzung und Form von Halbzeug - Teil 3: Chemische Zusammensetzung und Erzeugnisform.” 2013.
- [6] Y. Birol, “Effect of homogenisation cooling rate and press exit temperature on extrudability and T5 hardness of EN AW 6082 alloy,” *Mater. Sci. Technol.*, vol. 29, no. 12, pp. 1518–1521, 2013.
- [7] R. Hu, T. Ogura, H. Tezuka, T. Sato, and Q. Liu, “Dispersoid Formation and Recrystallization Behavior in an Al-Mg-Si-Mn Alloy,” *J. Mater. Sci. Technol.*, vol. 26, no. 3, pp. 237–243, 2010.
- [8] S. Tomovic-petrovic and O. Jensrud, “Extrusion of silicon-rich AlMgSi alloys,” *J. Mater. Process. Tech.*, vol. 212, no. 6, pp. 1437–1442, 2012.
- [9] a K. Gupta, D. J. Lloyd, and S. a Court, “Precipitation hardening in Al – Mg – Si alloys with and without excess Si,” *Science (80-. )*, vol. 316, pp. 11–17, 2001.
- [10] H. R. M. Semnani, “Precipitation Kinetics in Al-Alloys Observed by Dilatometry,” TU Wien, 2009.
- [11] P. Lang, E. Povoden-Karadeniz, A. Falahati, and E. Kozeschnik, “Simulation of the effect of composition on the precipitation in 6xxx Al alloys during continuous-heating DSC,” *J. Alloys Compd.*, vol. 612, pp. 443–449, 2014.
- [12] O. Reiso, “Extrusion of AlMgSi alloys,” in *Materials Forum*, 2004.
- [13] K. Strobel, J.-F. Nie, M. J. Couper, L. Sweet, and M. A. Easton, “Relating Quench Sensitivity to Microstructure in 6000 Series Aluminium Alloys,” *Mater. Trans.*, vol. 52, no. 5, pp. 914–919, 2011.
- [14] T. Sheppard, *Extrusion of Aluminium Alloys*. Dordrecht, Boston, London: Kluwer Academic Publishers, 1999.
- [15] M. Murayama and K. Hono, “Pre-precipitate clusters and precipitation processes in Al-Mg-Si alloys,” *Acta Mater.*, vol. 47, no. 5, pp. 1537–1548, 1999.
- [16] G. Gottstein, *Physikalische Grundlagen der Materialkunde*. .
- [17] F. J. Humphreys and M. Hatherly, *Recrystallization and Related Annealing Phenomena*, 2nd ed. Elsevier, 2004.
- [18] N. Parson, S. Barker, A. Shalanski, and C. Jowett, “Control of Grain Structure in Al-Mg-Si Extrusions,” *North*, pp. 11–22.
- [19] T. Weisz, H. Buken, D. Lukavsky, A. Falahati, T. Ebner, and E. Kozeschnik, “Rekristallisation in 6xxx Legierungen : Experiment und Modellierung.”
- [20] S. N. Samaras and G. N. Haidemenopoulos, “Modelling of microsegregation and homogenization of 6061 extrudable Al-alloy,” *J. Mater. Process. Technol.*, vol. 194, no.

- 1–3, pp. 63–73, 2007.
- [21] M. V Brant, D. C. Bone, and E. F. Emley, “Fumeless In-Line Degassing and Cleaning of Liquid Aluminum,” *JOM*, vol. 23, no. 3, pp. 48–53, 1971.
- [22] “Direct-Chill Casting.” [Online]. Available: <https://www.totalmateria.com/page.aspx?ID=CheckArticle&site=ktn&NM=384>. [Accessed: 04-Feb-2019].
- [23] A. von Starck, A. Mühlbauer, and C. Kramer, *Handbook of Thermoprocessing Technologies*. Essen: Vulkan-Verlag GmbH, 2005.
- [24] N. C. W. Kuijpers, F. J. Vermolen, C. Vuik, P. T. G. Koenis, K. E. Nilsen, and S. van der Zwaag, “The dependence of the  $\beta$ -AlFeSi to  $\alpha$ -Al(FeMn)Si transformation kinetics in Al-Mg-Si alloys on the alloying elements,” *Mater. Sci. Eng. A*, vol. 394, no. 1–2, pp. 9–19, 2005.
- [25] H. Hoffman, R. Neugebauer, and G. Spur, *Handbuch Umformen*. Carl Hanser Verlag GmbH & Co KG, 2012.
- [26] P. K. Saha, *Aluminium Extrusion Technology*. Ohio: ASM International, 2000.
- [27] K. Müller, *Grundlagen des Strangpressens*. Renningen-Malmsheim: expert verlag, 1995.
- [28] K. Laue and H. Stenger, *Strangpressen: Verfahren, Maschinen, Werkzeuge*. Düsseldorf: Aluminium-Verlag GmbH, 1976.
- [29] P. T. Moe, “Pressure and Strain Measurement During Hot Extrusion of Aluminium,” NTNU, 2005.
- [30] W. Hähnel, K. Gillmeister, and A. Krüger, “Temperatur-Management an Rezipienten in Aluminium-Strangpressen.” pp. 36–40, 2015.
- [31] S. Bingol, “The Decreasing of the Extrusion Time with Varying Ram Speed,” *Mater. Manuf. Process.*, vol. 30, no. 10, pp. 1185–1189, 2015.
- [32] “DIN EN 515:2017 Halbzeug - Bezeichnungen der Werkstoffzustände.” 2017.
- [33] “ASTM E112-10 Standard Test Methods for Determining Average Grain Size,” vol. 96, no. 2004. 2010.
- [34] “DIN EN ISO 643:2017 Stahl - Mikrophotographische Bestimmung der erkennbaren Korngröße.” 2017.
- [35] “DIN EN ISO 6506-1:2015 Metallische Werkstoffe - Härteprüfung nach Brinell.” 2015.
- [36] “DIN EN 60584-1:2013 Thermolemente - Thermospannungen und Grenzabweichungen.” 2013.
- [37] H. D. Baehr and K. Stephan, *Wärme- und Stoffübertragung*. 2013.
- [38] A. J. N. Khalif and I. R. A. Al mousawi, “Comparison of Heat Transfer Coefficients in Free and Forced Convection using Circular Annular Finned Tubes,” vol. 5, no. 4, pp. 194–204, 2016.
- [39] “Wärmeübergangskoeffizienten - Gase -Luft.” [Online]. Available: [https://www.schweizer-fn.de/stoff/wuebergang\\_gase/wuebergang\\_gase.php](https://www.schweizer-fn.de/stoff/wuebergang_gase/wuebergang_gase.php). [Accessed: 25-Oct-2018].
- [40] “Wärmeübergangskoeffizient.” [Online]. Available: <https://de.wikipedia.org/wiki/Wärmeübergangskoeffizient>. [Accessed: 31-Oct-2018].
- [41] T. Sheppard and A. Jackson, “Constitutive equations for use in prediction of flow stress during extrusion of aluminium alloys,” *Mater. Sci. Technol.*, vol. 13, no. 3, pp. 210–216, 1997.
- [42] T. Pettersen and E. Nes, “Recrystallization of an AlMgSi alloy after different modes of hot deformation,” *Metall. Mater. Trans. A Phys. Metall. Mater. Sci.*, vol. 34, no. 12, pp. 2717–2726, 2003.

## List of figures

<i>Figure 1: Quasi-binary phase diagram for AlMgSi-alloys [4].</i>	5
<i>Figure 2: MatCalc thermodynamic equilibrium computation of specific AW6082 alloy. The black dotted circle marks the temperature window where Mg-Si intermetallic phases are dissolved into solid solution.</i>	7
<i>Figure 3: Mg- and Si- contents for many 6xxx alloys. Empty box means no Cu in the alloy, filled box indicates Cu content [4].</i>	9
<i>Figure 4: Change of mechanical properties for naturally aged press profiles of AW6082 alloy [4].</i>	12
<i>Figure 5: Trend in hardness of an artificially aged AW6082 alloy, with and without prior natural ageing [4].</i>	12
<i>Figure 6: Relationship between strength and particle size for age-hardened alloys [16].</i>	13
<i>Figure 7: Temperature-time regime for whole extrusion process [12].</i>	16
<i>Figure 8: Vertical DC-casting scheme [22].</i>	17
<i>Figure 9: Configuration of a direct extrusion press: 1...feeder plate, 2...die, 3...backer, 4...die ring, 5...bolster, 6...pressure pad, 7...dummy block [26].</i>	20
<i>Figure 10: (a) Schematic of flowing material during extrusion. (b) Pressure profile of direct and indirect extrusion changing with ram displacement [26].</i>	22
<i>Figure 11: Principle of taper heating or variable ram speed for isothermal extrusion [26].</i>	24
<i>Figure 12: Friction components in direct extrusion plants [26].</i>	25
<i>Figure 13: Dimensions of billets and thermocouple positions for (a) AH1 – AH5 and (b) AH6 - AH10.</i>	28
<i>Figure 14: Cooling rates for billets from 450°C at ambient conditions with regression lines and corresponding equations.</i>	29
<i>Figure 15: Laboratory extrusion press.</i>	30
<i>Figure 16: Used die geometries: (a) RW-die, (b) W10-die, (c) W5-die and (d) QW-die.</i>	32
<i>Figure 17: Deformations of extruded products because of too high pre-heating temperature: (a) plugged RW-die with twisted extrudate and (b) rectangular extrudate distorted and out of dimension.</i>	33

<i>Figure 18: Embedded specimens for the RW-die (Left), the QW-die (middle), the W10-die (bottom right) and in not-extruded homogenized condition (top right).</i>	35
<i>Figure 19: Measured billet temperatures in comparison surface to core for varying furnace temperatures, test series AH1 – AH5.</i>	39
<i>Figure 20: Temperatures of billet surface and core for test series AH6 – AH10 at 600°C oven temperature.</i>	40
<i>Figure 21: Temperature deviations oven to core when heating the oven to: (a) 480°C and (b) 500°C.</i>	41
<i>Figure 22: Billet with thermocouples before (a) and (b) after first temperature test.</i>	42
<i>Figure 23: Billet geometry inside the container [26].</i>	50
<i>Figure 24: Cross-section polish of all dies, with billets being pre-heated to 480°C: (a) RW-die at 25x magnification, (b) QW-die at 12,5x magnification, (c) W5-die at 25x magnification and (d) W10-die at 12,5x magnification.</i>	51
<i>Figure 25: Comparison of grain elongation for extrudates of (a) W10-die, (b) QW-die and (c) W5-die at 25x magnification.</i>	52
<i>Figure 26: Hardness of products in the QW-form for thermal routes T1, T5 and T6 with different solution and ageing times.</i>	54
<i>Figure 27: Influence of pre-heating temperature on product hardness for RW-die.</i>	55
<i>Figure 28: Hardness for different pre-heating temperatures and thermal routes, measured from longitudinal- and from short transverse direction of RW-extruded product.</i>	55
<i>Figure 29: QW-product in T6 temper, with also recrystallized coarse grain in the inner section and just a small un-recrystallized section of fine grain in the center (a) and (b).</i>	57
<i>Figure 30: Light optical microscope pictures show dispersoids in (a) cast and homogenized form, (b) longitudinal section of extrudate and (c) cross section of extrudate. All figures were taken at 500x magnification.</i>	58

## List of tables

<i>Table 1: Numerical designation system for Al-alloys [3] [4].</i>	1
<i>Table 2: Composition of EN AW6082 billets in weight percent.</i>	4
<i>Table 3: Denomination and dimensions of all used die geometries.</i>	31
<i>Table 4: Overview to tested pre-heating temperatures and thermal routes.</i>	34
<i>Table 5: Parameters for grinding and polishing with preparation machine TegraPol-31.</i>	35
<i>Table 6: Temperature deviations for cube and billet during heating characterisation.</i>	42
<i>Table 7: Parameters used for calculation of the empirical heat transfer coefficient aluminium - air.</i>	44
<i>Table 8: Different types of heat generation calculated for diverse die geometries. This table also contains the geometrical data and flow stress for every die form.</i>	46
<i>Table 9: Flow stress for all die geometries at 480°C, according to individual strain rates.</i>	47
<i>Table 10: Extrusion ratios for different die geometries.</i>	48
<i>Table 11: Natural strain, strain rates and length of extrudates for different die geometries.</i>	49